Journal of Palaeogeography, 2025, 14(2): 391—412 (00387)

Available online at www.sciencedirect.com

ScienceDirect

journal homepage: http://www.journals.elsevier.com/journal-of-palaeogeography/

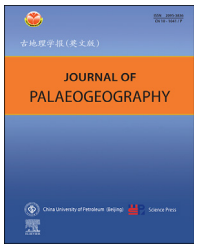

Research article

Giant paleo-landslides in the upper reaches of the Yellow River: Spatio—temporal distribution, and possible controlling factors

Yi-Qi Ji [a,b,c], *Sheng-Rui Su* [a,d,*], *Alessandro Simoni* [b], *Qiang-Bing Huang* [a,d]

[a] *School of Geological Engineering and Geomatics, Chang'an University, Xi'an 710054, Shaanxi Province, China*
[b] *Department of Biological, Geological and Environmental Sciences, University of Bologna, Via Zamboni 67 40126 Bologna, Italy*
[c] *Shaanxi Institute of Geo-Environment Monitoring (Shaanxi Geological Hazards Center), Xi'an 710054, Shaanxi Province, China*
[d] *Key Laboratory of Western China's Mineral Resources and Geological Engineering, Ministry of Education, Chang'an University, Xi'an 710054, Shaanxi Province, China*

Abstract A large number of giant paleo-landslides were found in the section from Lagan Gorge to Liujia Gorge, which is located in the upper reaches of the Yellow River. This area is located in the transition zone between the Qinghai—Tibet Plateau and the Loess Plateau with a semi-arid climate. The occurrence of lacustrine deposits suggests that some of the giant landslides ever blocked the river and landslide-dammed lakes have occurred in this area. The chronology of the giant landslide in the upper Yellow River was obtained and analyzed by optically stimulated luminescence (OSL) dating and established a chronological framework combining previous data. From the perspective of space, there are five major landslide clusters in the upper Yellow River. They are mainly located in the canyons at the junction of the Yellow River valley, and the center of every basins, which are inextricably linked to the unique sedimentary and tectonic environments of each basin. From the perspective of time, giant landslides also tend to occur during interglacial or glacial-to-interglacial transitions. Paleoseismicity and precipitation appear to be coupled and have competing relationships in their contribution to the formation of giant landslides.

Keywords Upper Yellow River, Giant paleo-landslides, Lacustrine deposits, River blocking, OSL dating, Genesis mechanism

Received 24 January 2024; revised 30 May 2024; accepted 30 December 2024; available online 8 February 2025

* Corresponding author. School of Geological Engineering and Geomatics, Chang'an University, Xi'an 710054, Shaanxi Province, China.
E-mail addresses: yiqiji12@chd.edu.cn (Y.-Q. Ji), shengruisu@163.com (S.-R. Su), alessandro.simoni@unibo.it (A. Simoni).
Peer review under responsibility of China University of Petroleum (Beijing).
https://doi.org/10.1016/j.jop.2024.12.006

1. Introduction

Because of the subduction of the Indian Plate to the Eurasian Plate, the Tibet Plateau has been rapidly uplifted since the Paleogene (Zhang *et al.*, 2000; Li *et al.*, 2015). The upper Yellow River is located at the northeastern margin of the Tibet Plateau, and the rapid uplift and river erosion has produced a highly active geomorphological evolution. Many giant paleo-landslides that are distributed along the steep slopes have drawn the attention of the engineering geological community (e.g., Lan *et al.*, 2022). Recent studies demonstrated that the river terraces along the upper reaches of the Yellow River are controlled by tectonics and climate (Guo *et al.*, 2018). Giant paleo-landslides, as parts of geomorphic archives, are the combined result of various effects (Yin *et al.*, 2014). However, until recently, our understanding about the region's tectonics, geomorphology, and paleoclimate was not detailed enough to make a connection between them and the giant paleo-landslides. The connection between tectonic activity, climate change, and surface process is a complex, multidisciplinary, and comprehensive research field and one of the hot issues for geoscientists around the world (e.g., Li *et al.*, 2015). Tectonic activity and paleoclimate are coupled at the surface, and topography is a response to tectonic activity, and its changes can also alter the climate of local regions (Wang *et al.*, 2008). The study of the spatial and temporal distribution of ancient landslides is influenced by active tectonics, paleoseismicity, climate change, and other geological factors, has become an important direction to explore and has been receiving attention from scientists from all over the world in the last two decades (Yin *et al.*, 2000). The triggering factors for the giant landslides in the Apennine region of northern Italy were mainly water pressure and seismic events (Soldati *et al.*, 2004; Sanchez *et al.*, 2010). The main cause of the multi-phase large-scale paleo landslides in the Three Gorges reservoir area is the paleoclimatic changes and neotectonic movements since the Quaternary (Li *et al.*, 2008). Landslide activity is concentrated in the wet phase due to abundant precipitation, and landslides can be triggered by strong earthquakes and extreme weather events (Chigira, 2002; Kumar *et al.*, 2019).

Fluvial geomorphology represents a valuable record of continental environments and has been widely used to demonstrate the dynamic interactions between tectonic activity and surface processes in the setting of global change (Cordier *et al.*, 2017). In the case of landslides which ever block the river, the geochemical composition of landslide deposits, and lacustrine sediments, are influenced by the composition of the source area, transport processes, and post-deposition weathering. The source of the deposits is usually determined by analyzing the geochemical composition of the sediments and by comparing the abundance and proportions of major elements in different samples (An *et al.*, 2012). Previous investigations of lacustrine deposits in the upper Jinsha River, as well as grain size and SEM analyses, have been used to explore the mechanism of giant landslide formation and the evolutionary history of the river section, comparing the top elevation information and the chemical and mineral compositions of the lacustrine sediments around the residual dams, the order of the demise of two dammed lakes was obtained (Li *et al.*, 2020, 2022). Similar studies in the upper reaches of the Yellow River are rare, despite their significance for the study of the evolutionary history of the river section including landslide blockages.

The research on giant paleo-landslides in the upper Yellow River mainly focuses on two aspects: spatio-temporal distribution pattern and genesis mechanism (e.g., Li *et al.*, 2011; Yin *et al.*, 2014; Zhou *et al.*, 2014; Guo *et al.*, 2020, 2022; Ji, 2024). The triggering factors are mainly concentrated in the two aspects of fault activities (earthquakes) and climate change (precipitation). The geological conditions of the upper Yellow River on the northeastern edge of the Qinghai—Tibet Plateau are very complex. Under the synergistic effect of tectonic activity and climate, many giant paleo-landslides were formed in the section from Lagan Gorge to Liujia Gorge (Yin *et al.*, 2014).

This study relies on field investigation and aerial photograph interpretation to identify and map giant paleo-landslides in the upper Yellow River. Both landslide and lacustrine deposits were sampled to estimate the ages of several giant landslides through OSL dating. We combine our results with those obtained to establish a summary framework that describes the chronology of landslide formation and their distribution along the river catchment (Li *et al.*, 2011; Zhou *et al.*, 2014). The main objectives of this study are 1) to map the giant paleo-landslides and landslide-dammed lakes in the upper Yellow River; 2) to describe the main types of deposits of giant paleo-landslides; 3) to analyze the spatial and temporal distribution of giant paleo landslides to get some insight into their formation mechanism.

2. Regional setting

2.1. Geomorphology

The river section from Lagan Gorge to Liujia Gorge is located in the upper reaches of the Yellow River (Fig. 1), with an elevation of 1732 m—2632 m and a length of 388 km (Ji *et al.*, 2022), which is located in the transition zone between the Loess Plateau and the Qinghai—Tibet Plateau, where the Lajishan Fault Zone and the West Qinling Fault are distributed. The valley is cut by the mainstream of the Yellow River in turn, and several giant landslides blocking the river have occurred in the basin since the Late Pleistocene, forming landslide-dammed lakes of different sizes, and the lacustrine deposits are distributed on both sides of the wide Yellow River valley (Guo *et al.*, 2015, 2020, 2022).

The Yellow River passes through the Gonghe Basin, Guide Basin, Jianzha Basin, Xunhua Basin, and Linxia Basin in turn. Here, the basin is a basic geomorphologic unit separated by mountain ranges. The terrain is high in the west and low in the east, with mountains stacked up horizontally and confronting each other in the north and the south. The landform of the study area is mainly divided into plain landforms, hilly landforms, mountainous landforms, and layered landforms. The geomorphology of the upper reaches of the Yellow River is a response to the regional tectonic and tectonic activities, and the paleoclimate shapes the land surface to a certain extent.

2.2. Geological structure and stratigraphic lithology

The study area is located at the border between the West Qinling Block and the South Qilian Block, spanning two major geomorphological units. The geological structure is relatively complex, bounded by the deep and large fracture zone of the northern margin of the Qinghai Nanshan—West Qinling, with the South Qilian fold belt to the north and the Qinling fold system to the south. The tectonic lines are mainly NW—NWW orientated directions, forming a multi-layered and complex tectonic pattern. The main faults in the area are the NW—NNW-oriented Lajishan Fault Zone (LJFSZ) and the NW-oriented West Qinling Fault (WQLF).

The Qinghai—Tibet Plateau has been uplifted since 45 ka, and the rate of uplift has intensified significantly since the Quaternary. Uplift movements at different times have profoundly influenced the shaping of regional topography and landscape, the formation of large rivers, and the evolution of structural surfaces. In the late Pliocene, the plateau surface was only

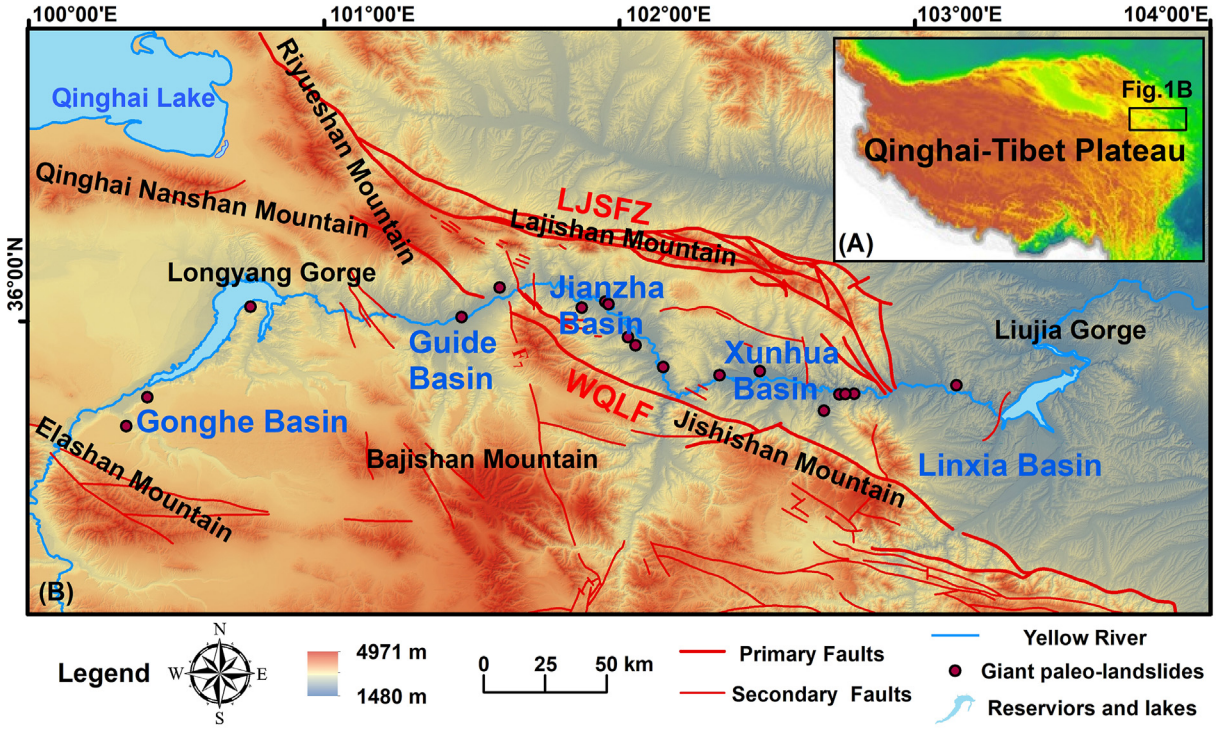

Fig. 1 **A)** Map of the Qinghai—Tibet Plateau and the location of the study area; **B)** The regional geomorphic map of the study area. LJSFZ = Lajishan Fault Zone; WQLF = West Qinling Fault.

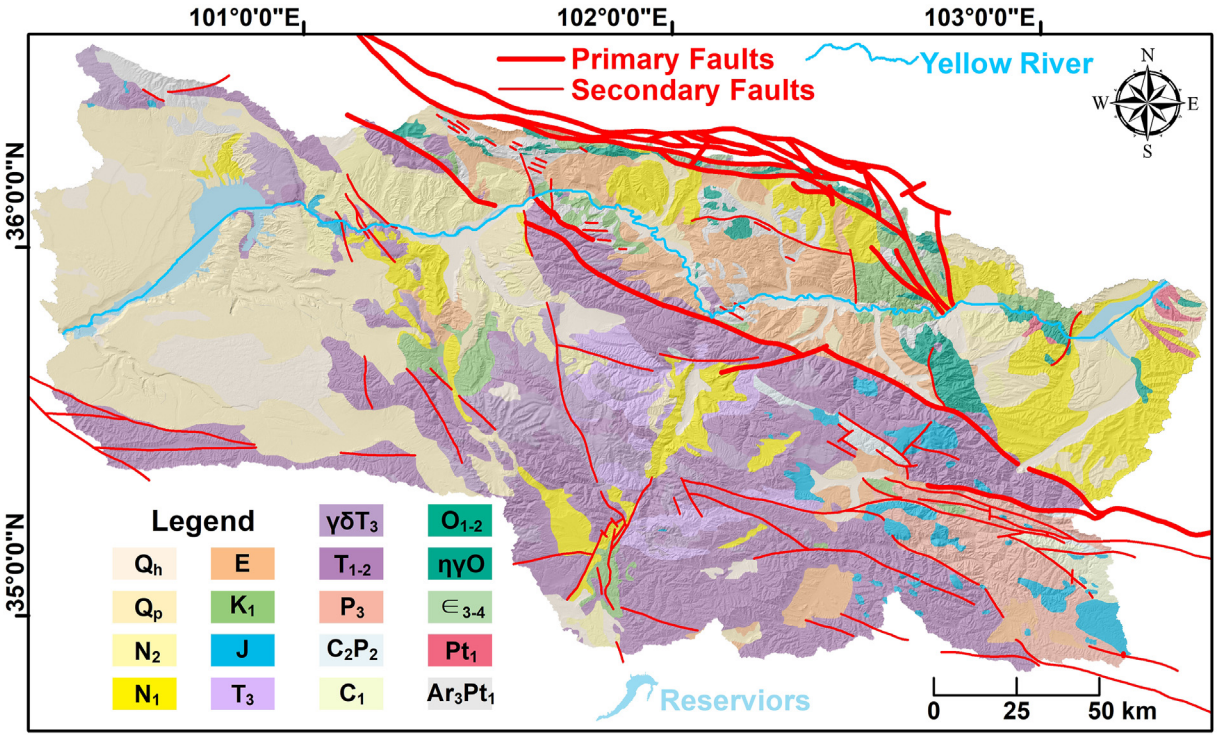

Fig. 2 The regional geological map (obtained from http://www.ngac.org.cn), displays the main strata and the major regional faults (Annotations: Ar_3Pt_1—Mesoarchean and the Paleoproterozoic; Pt_1—Paleoproterozoic; $\in_{3\text{-}4}$—Upper Cambrian; ηγO—Monzonitic granite in the Ordovician; $O_{1\text{-}2}$—Lower to Middle Ordovician; C_1—Lower Carboniferous; C_2P_2—Middle Carboniferous and Middle Permian; P_3—Upper Permian; $T_{1\text{-}2}$—Lower to Middle Triassic; γδT_3—Granodiorite in Upper Triassic; T_3—Upper Triassic; J—Jurassic; K_1—Lower Cretaceous; E—Eocene; N_1—Lower Neogene; N_2—Upper Neogene; Qp—Pleistocene; Q_h—Holocene).

1000 m above sea level, but now it is more than 4500 m above sea level, and the cumulative uplift has reached 3500 m—4000 m. Rapid uplift reactivated some faults in the area, accelerated the cutting of riverbanks, and increased the free face of landslides, which is the factor of the geodynamics for the intensification of the landslides in this stage. The several uplifts of the Qinghai—Tibet Plateau resulted in the formation of normal faults around the river valleys, and landslides occurred where the critical surfaces were located; during uplift, deep and large fractures, and tension cracks were formed, which induced landslides (Yin *et al.*, 2016).

Neotectonic activity often controls regional landscapes (Ji *et al.*, 2021). There are frequent neotectonic activities in the study area, and regional tectonics is the background for the formation of giant landslides, which determines the group occurrence and susceptibility of giant landslides, thus basins with active tectonic activities tend to have more giant landslides, and the controlling factors of these giant landslides come from the internal geological stress, which also determines the location of the giant landslides (Ji *et al.*, 2022). The giant landslides are distributed in five major sedimentary basins. The exposed strata are mainly Triassic thick clastic rocks, and Quaternary sediments including loess, fluvial sediments and lacustrine deposits and red sandstones (Fig. 2). The sedimentary sequence exposed along the upper Yellow River is characterized by past interactions between climate and surface processes in the cold and semi-arid regions of the northeastern Qinghai—Tibet Plateau.

The stratigraphy of the study area is relatively complete, and the main strata are the Permian, Triassic, Cretaceous, Paleogene (Eocene), Neogene, and Quaternary (Fig. 2). The most widely distributed is the Triassic strata, with sandstones and slate, which are the main rocks of the Qinghai—Tibet Plateau, followed by Paleogene and Neogene, with mostly mudstones, sandstones, muddy sandstones, and conglomerates. The Quaternary strata are also widely distributed in the study area, which are divided into: the Pleistocene (Q_P) and the Holocene (Q_h).

2.3. Climate characteristics

The section is located in a semi-arid to arid zone, with a typical plateau continental dry climate, scarce rainfall, long sunshine hours, high radiation levels, low

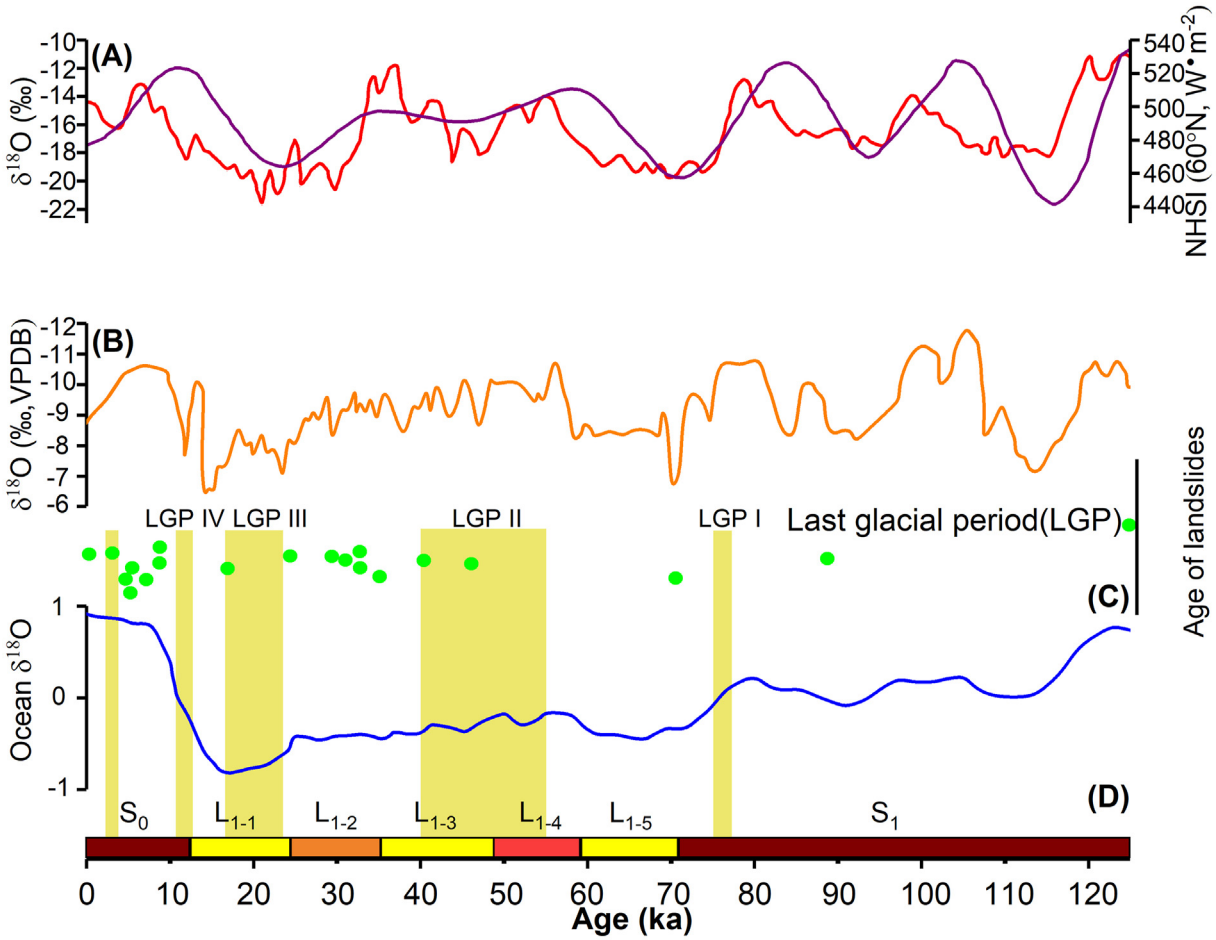

Fig. 3 **A)** $\delta^{18}O$ record from the Guliya ice core (red curve) and summer solar insolation at 60°N (purple curve); **B)** Speleothem $\delta^{18}O$ record from the Sanbao Cave (orange curve); **C)** Chronology of giant landslides (green dots); **D)** $\delta^{18}O$ record of ocean sediments (blue curve). S_0 and S_1 denote Holocene paleosol and Late Pleistocene paleosol horizons, respectively; L_{1-1}, L_{1-3}, and L_{1-5} denote loess horizons; L_{1-2} and L_{1-4} denote weakly developed paleosol horizons (modified from Martinson *et al.*, 1987; Yao *et al.*, 1997; Wang *et al.*, 2008; Qin *et al.*, 2009).

temperatures, large temperature differences between day and night, indistinguishable seasons, cold winters and long cool summers. The average annual precipitation is 316—436 mm/yr, the average annual temperature is 2.2°C—8.5 °C, and the average annual potential evaporation is 2100—2200 mm (Ji *et al.*, 2022). The Qinghai—Tibet Plateau is the highest and youngest major plateau in the world. Its size and height have a significant impact on atmospheric circulation, and its uplift has altered the monsoon system in East Asia and globally, leading to the generation of monsoon winds and the branching of westerly winds bypassing the flow, which has a significant impact on the environment of East Asia as well as on the climate of the Northern Hemisphere (Shi *et al.*, 1999).

The climatic frames are presented mainly by the Guliya ice core (Yao *et al.*, 1997). Paleoclimate records from the Guliya ice core on the Qinghai—Tibet Plateau and the Malan Loess on the Loess Plateau, and $\delta^{18}O$ records from the Sanbao Cave are thought to be similar to those from the upper reaches of the Yellow River (Fig. 3). Although there is a lack of paleoclimate studies in the region, it can be argued that the sequence of global climate changes caused by regional and global events during this period is similar to that reconstructed by other researchers for the Qinghai—Tibet Plateau and the Loess Plateau.

3. Methods

In this study, field observations, aerial photographs, and various experiments on landslide deposits and OSL dating experiments were used to explain the mechanisms of giant landslide formation. Basic data on the region including engineering geological conditions, tectonic activity, geomorphological features, and previous dating results were extensively collected.

Finally, detailed field investigations were carried out along the upper Yellow River in September 2020, June 2021, and August 2022, and lacustrine deposits, landslide deposits, and slope deposits along the Yellow River were tested for OSL dating to assess the chronology of the paleo-landslides. We used the Shuttle Radar Topography Mission (SRTM) data for topographic information because of its higher vertical accuracy and better vegetation penetration compared to the Advanced Spaceborne Thermal Emission and Reflection Radiometer Global Digital Elevation Model (ASTER-GDEM) (Liu *et al.*, 2021). The genesis mechanism of the giant landslides in the region was finally determined.

3.1. Field investigation and sampling

Giant landslides in different basins of the upper Yellow River have widely different breeding backgrounds, and their spatial distribution characteristics, developmental features, and genesis mechanisms are all different. We investigated each giant landslide in the study area, took photos and videos of the whole landscape of giant landslides with a small unmanned aerial vehicle (UAV), combined with remote sensing interpretation to determine the boundary of each giant landslide, focused on investigating the leading edge of each giant landslide, paid attention to whether there are signs of deformation, and collected some basic information on-site by using hand-held GPS, rangefinders, and compass surveys. Normally, the giant landslides in the same basin have similar geological structures, stratigraphic lithology, and topographic and geomorphological conditions.

Four typical giant landslides in different basins, the Mangla River landslide (Fig. 4A) in Gonghe Basin, the Xijitan landslide (Fig. 4B) in Guide Basin, the Xiazangtan landslide (Fig. 4C) in Jianzha Basin, and the Shangen landslide (Fig. 4D) in Xunhua Basin, were selected for detailed investigation. The Quaternary sedimentary construction in the Gonghe Basin mainly consists of the Lower Pleistocene lacustrine deposits, which is unconformably overlain the Neoproterozoic Linxia Formation. There are 3 giant landslides, and their residual volumes range from 100 to 300 million m^3. The stratigraphy around the Guide Basin is dominated by Neogene and Quaternary strata, and the rock types are sand slate and sandstone with sand conglomerate. The number of giant landslides in the Guide Basin is two, and their residual volume ranges from 100 to 800 million m^3. The Quaternary sedimentary construction in the Jianzha Basin consists of the Early Pleistocene lacustrine layers and the Holocene alluvial layers, unconformably overlain the Neoproterozoic Linxia Formation, and there are 7 giant landslides in the Jianzha Basin with a maximum volume of 1.5 billion m^3. In the Xunhua Basin, there are 6 giant landslides, and their Cenozoic sedimentary layers are typical red layers of the plateau, which are mainly buried giant thick bedded mudstones or siltstones, with a residual volume of between 100 and 200 million m^3.

Based on the fieldwork, the spatial distribution of giant landslides was characterized. In addition, to understand the type of sediment and the age of the giant landslide, samples from different layers were collected for various laboratory tests and analyses. The depth of sampling is 30 cm. A total of 32 sediment samples were collected, including 6 samples from the Gonghe Basin, 4 samples from the Guide Basin, 14 samples from the Jianzha Basin, and 8 samples from the Xunhua Basin; the collection sites were located 0—30 m from the riverbanks, and all the sampling sites were avoided from the areas of human activities, to ensure that the samples were not affected by human factors. The sampling locations are shown as red stars and yellow hexagons in Fig. 5. Specific information on the samples is shown in Table 1.

3.2. OSL dating

To reconstruct the chronological sequence of giant paleo-landslides, geochronological control is required. OSL dating has been widely used in landslide dating and has been proven to be an effective method in the upper reaches of the Yellow River (Guo *et al.*, 2015, 2020, 2022). After a long time and careful investigation, we found that it was difficult to find samples for ^{14}C dating in the landslide deposits in the study area, and it was also difficult to find in-situ organic matter contemporaneous with the landslide event, so the ^{14}C dating method was not feasible and the ^{14}C dating results of the samples from the northeastern Tibet Plateau, which were more than 25,000 years old, might need to be re-studied because of underestimation, however, the results obtained by using OSL dating were more in agreement with stratigraphy and climate records (Huntley and Prescott, 2001). A steel tube with a length of 30 cm and an inner diameter of 5 cm was inserted vertically into the cleaned section and sampled to a depth of 30 cm. When the sample filled the entire steel tube, it was removed and sealed with tin foil to avoid solar radiation. Samples were taken primarily at the interface between landslide deposits and the overlying interface or at the interface between lacustrine sediments. OSL samples were measured at the Key Laboratory for Integrated and Efficient Utilization of Salt Lake Resources, Qinghai Salt Lake Research Institute, Chinese Academy of

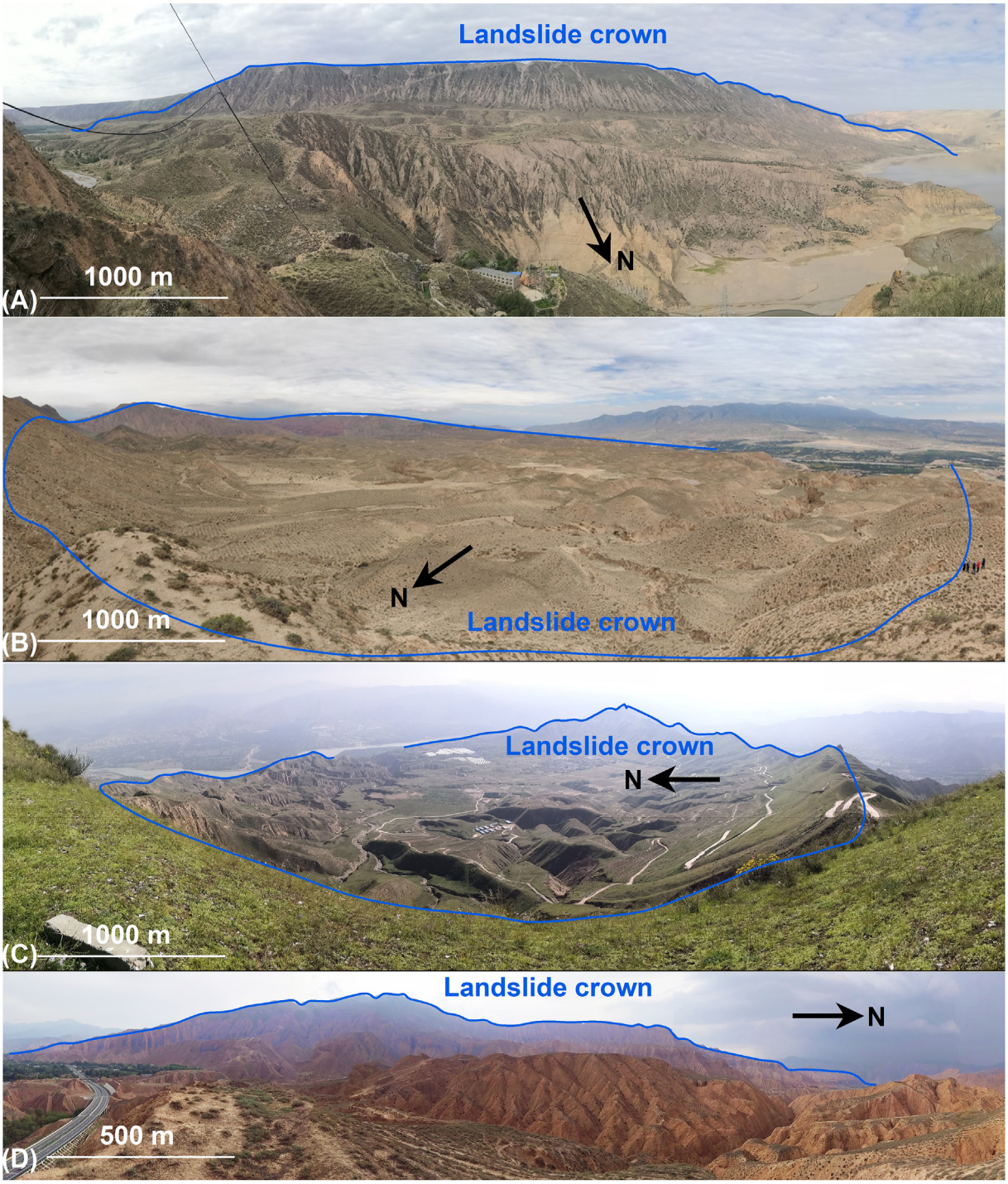

Fig. 4 Photographs of typical giant landslides. **A)** Mangla River landslide in Gonghe Basin; **B)** Xijitan landslide in Guide Basin; **C)** Xiazangtan landslide in Jianzha Basin; **D)** Shangen landslide in Xunhua Basin.

Sciences. The interior of the OSL samples was extracted from 30 cm long tubes. Pretreatment of the samples and experimental tests (water content and equivalent dose) were performed in the laboratory. Quartz minerals were selected for OSL dating, and the single-aliquot OSL (SAR) method was used.

3.3. Grain size analysis

Landslides can be meaningfully interpreted in the sedimentary record (Shanmugam, 2015). Grain-size measurement reflects the layering of the overlying lacustrine sediments and thus can further confirm the

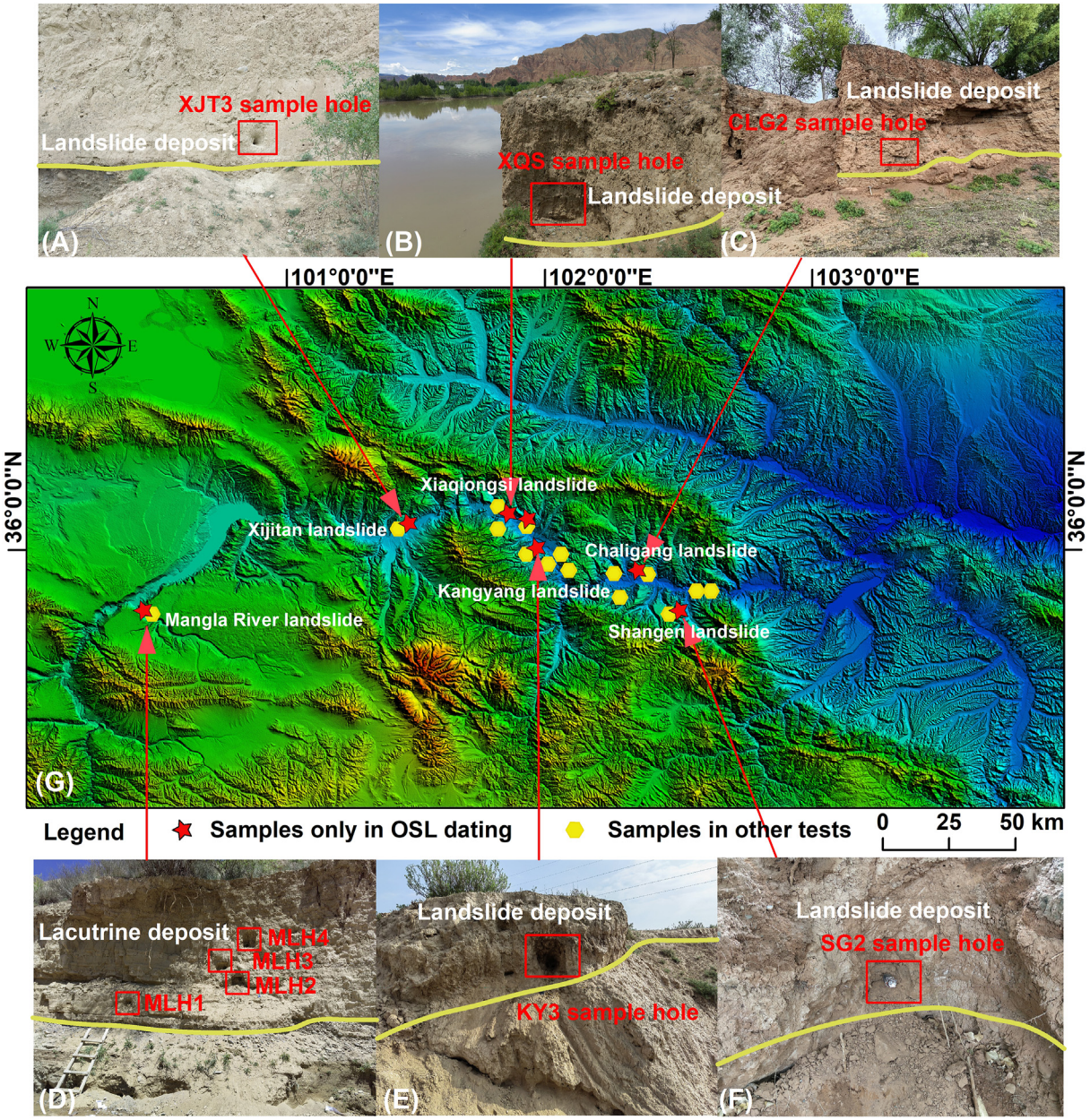

Fig. 5 Representative giant landslide sample distribution map in the upper reaches of the Yellow River. **A)** Photograph of sampling XJT3 in Xijitan landslide; **B)** Photograph of sampling XQS in Xiaqiongsi landslide; **C)** Photograph of sampling CLG2 in Chaligang landslide; **D)** Photograph of sampling MLH1—MLH4 in Mangla River landslide; **E)** Photograph of sampling KY3 in Kangyang landslide; **F)** Photograph of sampling SG2 in Shangen landslide; **G)** Plane view of the study area showing the specific sampling locations.

field stratigraphic identification and correlation between the lacustrine sediments. The grain size analysis was carried out at the Open Research Laboratory of Geotechnical Engineering, Ministry of Natural Resources, Chang'an University, using a Bettersize 2000 double-lens laser grain size distribution instrument. After pretreatment of the sample, slowly adding the sample to the instrument until the shading rate is maintained at 15%—20%, at this time you can get the best experimental test results; instrument with ultrasonic dispersion of the sample for 5—6 min, you can get the cumulative particle size distribution, the interval particle size distribution (data and curves), the median diameter, the weight of the average ratio, the specific surface area, etc. When you get the computer output of the experimental data, the experiments are completed. Grain size parameters (mean grain size, standard deviation, skewness, and kurtosis) were calculated for different sediments and used to determine depositional environments (Folk and Ward, 1957).

Table 1 Detailed information of the representative giant landslide samples for testing.

Sample	Location	Elevation/m	Type	Depth/cm	Test
MLH1	100°26′5″E 35°46′1″N	2664.38	Lacustrine deposit	30	OSL + Grain + XRF
MLH2	100°26′5″E 35°46′1″N	2665.38	Lacustrine deposit	30	OSL + Grain
MLH3	100°26′5″E 35°46′1″N	2665.98	Lacustrine deposit	30	OSL + Grain
MLH4	100°26′5″E 35°46′1″N	2667.18	Lacustrine deposit	30	OSL + Grain + XRF
MLH5	100°26′6″E 35°46′0″N	2680.90	Slope deposit	30	OSL + Grain
MLH6	100°26′6″E 35°46′0″N	2681.40	Slope deposit	30	OSL + Grain + XRD + XRF
XJT1	101°27′5″E 36°7′26″N	2552.23	Slope deposit	30	Grain
XJT2	101°27′6″E 36°7′25″N	2554.36	Slope deposit	30	Grain + XRF
XJT3	101°27′2″E 36°3′44″N	2157.44	Landslide deposit	30	OSL + Grain + XRD + XRF
XJT4	101°27′2″E 36°3′40″N	2155.46	Landslide deposit	30	Grain + XRD
XQS	101°51′35″E 36°6′57″N	2018.66	Landslide deposit	30	OSL + Grain + XRD + XRF
SGTD	101°54′36″E 36°5′45″N	2024.12	Slope deposit	30	OSL + Grain + XRD + XRF
TSC1	101°50′31″E 36°6′27″N	2042.76	Landslide deposit	30	Grain + XRD + XRF
TSC2	101°50′28″E 36°7′3″N	2038.88	Landslide deposit	30	Grain
KY1	101°55′50″E 36°3′44″N	2524.65	Slope deposit	30	Grain
KY2	101°56′47″E 35°59′42″N	2478.19	Slope deposit	30	Grain + XRD + XRF
KY3	101°57′43″E 35°59′43″N	2074.37	Landslide deposit	30	OSL + Grain + XRF
XZT1	101°57′9″E 35°58′27″N	2779.94	Slope deposit	30	Grain
XZT2	101°58′57″E 35°58′57″N	2260.33	Landslide deposit	30	Grain + XRD + XRF
XZT3	101°59′40″E 35°59′52″N	1974.94	Landslide deposit	30	Grain + XRF
DHL1	102°4′0″E 35°55′26″N	2128.13	Slope deposit	30	Grain
DHL2	102°3′59″E 35°55′31″N	2110.58	Landslide deposit	30	Grain + XRD + XRF
DHL3	102°4′4″E 35°55′26″N	2162.41	Landslide deposit	30	Grain
SZ	102°4′59″E 35°55′27″N	2101.37	Landslide deposit	30	Grain + XRD + XRF
TJXT	102°14′8″E 35°53′11″N	1907.36	Landslide deposit	30	Grain + XRD + XRF
DZNG	102°17′16″E 35°50′53″N	1958.25	Landslide deposit	30	Grain + XRD + XRF
GLG1	102°21′5″E 35°53′25″N	1876.36	Lacustrine deposit	30	Grain
GLG2	102°21′3″E 35°53′27″N	1889.59	Landslide deposit	30	OSL + Grain + XRD + XRF
SG1	102°33′6″E 35°46′37″N	2008.56	Slope deposit	30	Grain + XRF
SG2	102°33′4″E 35°46′35″N	2013.24	Landslide deposit	30	OSL + Grain + XRD + XRF
GLB	102°36′46″E 35°49′47″N	1832.85	Landslide deposit	30	Grain + XRD + XRF
MDX	102°38′15″E 35°49′46″N	1855.55	Landslide deposit	30	Grain + XRD + XRF

3.4. X-ray diffraction (XRD) analysis

All samples for this experiment were conducted in the Laboratory of Mineralization and Dynamics, Key Laboratory of Western Mineral Resources and Geological Engineering, Ministry of Education, Chang'an University. The mineral fractions of sediment samples were determined by the X-ray diffraction (XRD), and 15 samples were selected for the test separately. The test instrument was an XRD-6100 X-ray Powder Diffractometer. Take a small amount of sample with a medicine spoon and place it in the original aluminum sample sheet, pad it with weighing paper, and press the sheet with a glass plate, ensure the surface of the sample is flat after pressing, and blow off the excess sample with a dropper to ensure the cleanliness outside the sample tank. Open the door of the main unit, insert the sample into the sample holder of the main unit, close the door of the main unit, set the instrument conditions and sample name, and then click the start button to start the sample test, the sample holder keeps rotating until the test is completed, and the computer automatically draws the powder crystal X diffraction pattern of the sample in about 10 min. Finally, import the generated file into MDI Jade6, and Jade will analyze the main phases of the sample.

3.5. X-ray fluorescence (XRF) analysis

The major elements of sediments in different regions have different distribution patterns, which are caused by the geochemical composition of sediments influenced by the composition of source areas, transport processes, and weathering after the depositional period. The sedimentation histories of different river sections in different basins have great differences, so the analysis of the geochemical composition of sediments, the abundance of major elements, and the ratio of elements can be used to identify the source of sediments and can invert the process at the time of landslide occurrence. All samples for this experiment were collected in the Laboratory of Mineralization and Dynamics, Key Laboratory of Western Mineral

Resources and Geological Engineering, Ministry of Education, Chang'an University, and the major elemental contents of sediment samples were determined by X-ray fluorescence (XRF). Firstly, about 10 g of samples were selected and placed in a mortar, grounded to a size of 200 mesh, sieved out with a standard sieve of 0.075 mm, placed in a kraft paper bag, and dried in an oven at 40 °C for 72 h. The test instrument was an XRF-1800 sequential scanning X-ray Fluorescence Spectrometer manufactured by Shimadzu Corporation, Japan, with an error of <5% in elemental determination.

4. Results

4.1. Chronology of the giant landslide

The dating results of a total of seven landslides were obtained and combined with the previous publications (Li *et al.*, 2011; Zhou *et al.*, 2014; Guo *et al.*, 2015, 2022), and then the chronology of the giant landslides in the upper Yellow River was summarized (Table 2).

The samples have a good decay of their photoluminescence signals before deposition. The dispersion of all the samples in this test is less than 25%, and it is feasible to use the arithmetic mean model. Here, we've newly dated four giant landslides. The bottom of the lacustrine sediment layer opposite the Mangla River landslide was dated at 18.4 ka, which represents the time from which the dammed lake was deposited and when the landslide occurred. Dating samples were obtained at the interface between the Yellow River terrace and the landslide deposits, the results show that the Xiaqiongsi landslide occurred at 38.2±4.0 ka. The Shangen landslide was formed at 32.0±3.4 ka and the Chaligang landslide occurred at 48.5±4.2 ka, and the dating samples were obtained at the boundary between the landslide deposit and the original stratigraphy. These dating results are consistent with the actual situation.

4.2. Characteristics of grain size distribution

The grain size distribution curves for all types of sediments are shown in Fig. 6. There are two main types of curves, double and triple peaks. As the frequency curve of the grain size distribution is multi-peaked, it indicates that the deposit was involved in multiple deposition or transport processes. The Y-values of the 32 samples were greater than −2.74 except for the MLH2 and MLH3 samples. The grain size parameters and Y-values of the samples are shown in Table 3. The sediments of the Gonghe Basin are typical lacustrine deposits as well as wind-induced deposits. The samples from the Xijitan landslide in the Guide Basin are typical fluvial sediments. The Jianzha Basin has mainly wind-formed and fluvial sediments, and the Xunhua Basin has mainly fluvial and lacustrine deposits. Some of the samples show triple peaks in the

Table 2 Detailed information of the studied 19 giant landslides in the upper reaches of the Yellow River.

No.	Landslide	Slope angle (°)		Slope direction (°)	Distance to faults (km)	Area (km^2)	Conventional age (ka)	Basin
		Scarp	Deposit					
1	Mangla River	33.86	10.00	32	16.1	11.45	18.6±2.7	Gonghe Basin
2	Baicitan	29.34	1.56	315	26.7	17.20	5[a]	Gonghe Basin
3	Chana	32.82	2.41	319	/	13.83	0.08[a]	Gonghe Basin
4	Xijitan	22.71	3.51	185	0.0	24.31	9.6±0.8	Guide Basin
5	Ashigong	12.79	9.22	114	5.2	22.87	40.3±2.7[a]	Guide Basin
6	Xiaqiongsi	30.55	9.30	180	/	7.48	38.2±4.0	Jianzha Basin
7	Shenguotan	38.93	12.84	219	/	3.78	24±2[a]	Jianzha Basin
8	Dehenglong	/	4.61	241	9.8	8.58	89±8[a]	Jianzha Basin
9	Suozi	/	4.81	240	8.8	10.91	71±6[a]	Jianzha Basin
10	Tangsecun	18.33	11.73	50	5.2	12.66	32.9±2.4[a]	Jianzha Basin
11	Kangyang	31.41	9.79	29	11.3	20.01	10.1±0.9; 33.2±2.5[a]	Jianzha Basin
12	Xiazangtan	63.86	5.56	78	10.9	15.50	49±5; 28±3[a]	Jianzha Basin
13	Tangjiaxiantan	/	5.98	148	5.7	15.70	124.87±10.31[a]	Xunhua Basin
14	Chaligang	/	2.59	176	12.5	22.98	48.5±4.2	Xunhua Basin
15	Shangen	/	6.07	78	10.6	10.69	32.0±3.4	Xunhua Basin
16	Maerpodong	35.48	27.64	53	9.6	1.06	9.1±0.04[a]	Xunhua Basin
17	Gelongbu	/	18.88	340	8.1	1.61	9.1[a]	Xunhua Basin
18	Mendaxiang	/	14.96	13	6.7	1.34	3.7[a]	Xunhua Basin
19	Badashan	13.98	6.62	232	13.8	1.32	4.6±0.4[a]	Linxia Basin

[a] Stands for OSL dating age from other studies.

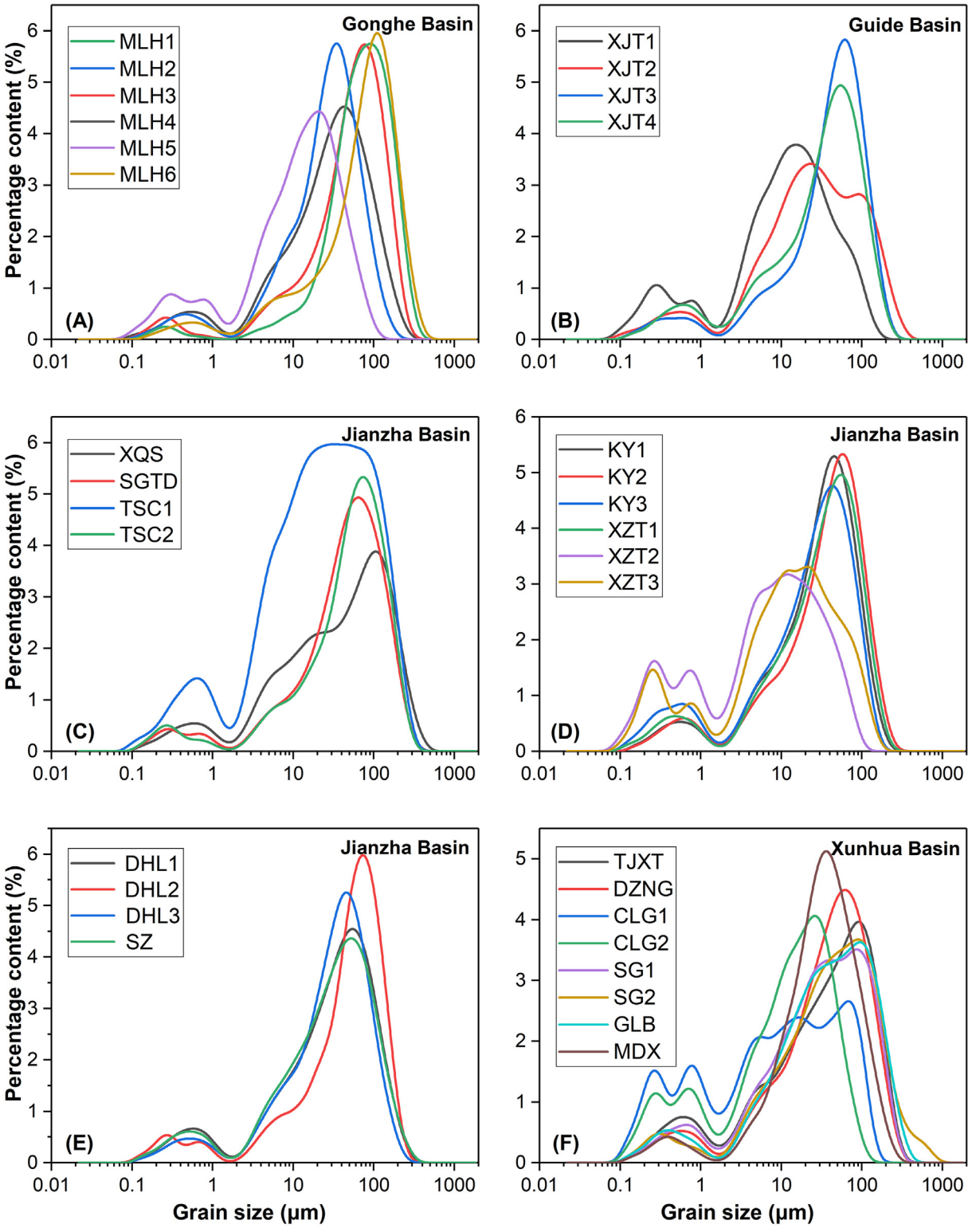

Fig. 6 Grain size distribution characteristics of the samples from the deposits in **A)** Gonghe Basin; **B)** Guide Basin; **C—E)** Jianzha Basin; **F)** Xunhua Basin.

Table 3 The grain size parameters and Y-values of the representative samples.

Sample	MS (ϕ)	σ (ϕ)	SK	KG	Y
MLH1	3.86	1.81	0.35	2.02	3.88
MLH2	5.41	1.81	0.37	1.55	−3.19
MLH3	4.40	1.60	0.36	1.25	−3.05
MLH4	5.30	2.09	0.34	1.35	0.69
MLH5	4.07	2.34	0.53	2.01	10.91
MLH6	4.20	2.59	0.57	1.96	14.81
XJT1	6.63	2.34	0.27	1.31	0.11
XJT2	5.39	2.32	0.19	1.20	4.06
XJT3	4.81	1.95	0.45	1.61	0.99
XJT4	5.30	2.20	0.45	1.27	2.00
XQS	4.94	2.42	0.34	1.06	6.65
SGTD	4.63	2.05	0.39	1.55	2.95
TSC1	5.55	2.36	0.20	1.09	3.74
TSC2	4.51	2.05	0.43	1.58	3.47
KY1	5.26	1.95	0.41	1.40	−1.24
KY2	5.02	2.02	0.43	1.44	0.76
KY3	5.67	2.21	0.43	1.32	1.05
XZT1	5.21	2.10	0.42	1.38	1.13
XZT2	7.64	2.66	0.29	0.85	1.00
XZT3	6.96	2.74	0.33	1.18	6.00
DHL1	5.19	2.16	0.38	1.34	2.05
DHL2	3.35	2.21	0.12	1.03	9.07
DHL3	5.14	1.90	0.37	1.45	−1.20
SZ	5.23	2.16	0.36	1.32	2.01
TJXT	5.18	2.45	0.38	1.12	6.46
DZNG	4.94	2.14	0.37	1.35	2.80
GLG1	7.17	2.95	0.22	0.76	8.51
GLG2	7.06	2.54	0.43	1.09	1.07
SG1	5.17	2.31	0.29	1.16	4.23
SG2	4.80	2.32	0.29	1.26	6.08
GLB	4.89	2.30	0.29	1.26	5.39
MDX	5.07	1.79	0.26	1.47	−2.15

Where ϕ is the converted sediment grain size; MS is the mean grain size; σ is the standard deviation; SK is the skewness; and KG is the kurtosis. If the calculated value Y < −2.74, the deposit is attributed to wind-induced deposition.

grain size curves, indicating a complex sedimentary genesis with wind, river, and lacustrine sediments.

4.3. Major element characteristics

The XRD 3D waterfall diagram of deposits is shown in Fig. 7. The stratigraphy of the study area is dominated by sedimentary strata containing Paleocene—Lower Quaternary mudstones, sandstones, and argillaceous sandstones. The mineralogical compositions of the accumulations in the study area, as revealed by XRD, are mainly clay minerals dominated by kaolinite and chlorite, and non-clay minerals dominated by detrital minerals, such as quartz, feldspar, calcite, and mica.

The major element contents (wt. %) of 21 samples are shown in Table 4. SiO_2 and Al_2O_3 are the most abundant major elements in the samples from the Yellow River section. The major element content of SiO_2 ranged from 53.17 wt. % to 68.97 wt. % with an average of 60.15 wt. %, Al_2O_3 ranged from 9.48 wt. % to 15.07 wt. % with an average of 11.41 wt. %, followed by CaO and TFe_2O_3 with contents of 4.11 wt. %—11.85 wt. % (average 7.86 wt. %) and 2.94 wt. %—5.59 wt. % (average 3.90 wt. %). Comparatively other major elements have lower contents, such as MgO (1.59 wt. %—3.05 wt. %, average 2.41 wt. %), K_2O (1.75 wt. %—2.99 wt. %, average 2.25 wt. %), Na_2O (1.40 wt. %—3.40 wt. %, average 1.93 wt. %), TiO_2 (0.52 wt. %—0.74 wt. %, average 0.61 wt. %), P_2O_5 (0.09 wt. %—0.20 wt. %, average 0.15 wt. %) and MnO (0.02 wt. %—0.11 wt. %, average 0.07 wt. %). The contents of major elements in slope deposits are different from those in lacustrine deposits, especially contents of Al_2O_3, Fe_2O_3, MgO, Na_2O and TiO_2, which suggests that the lacustrine deposits are not from local areas. Some scholars used the SiO_2/Al_2O_3 ratio as an index of maturity for detrital deposits because the ratio increases as quartz is progressively concentrated at the expense of less resistant phases during weathering, transport, or recycling (e.g., Roser and Korsch, 1988, 1999). The greater the maturity, the longer the distance that the deposit was transported. The maturity is calculated by ratios between the contents (wt. %) of SiO_2 and the contents (wt. %) of Al_2O_3 (Roser and Korsch, 1988, 1999), and its value of each sample are shown in Table 4.

The maturity of the lacustrine deposits is mostly greater than 4.3, ranging from 4.29 to 6.69. The Fe_2O_3 content of the sediments in the basin fluctuates from 3.06 wt. % to 5.59 wt. %, with the highest value occurring in the Xiazangtan landslide deposits in the Jianzha Basin, and the second highest value occurring in the deposits of the Gelongbu landslide and the Mendaxiang landslide, which are distributed in the Jishixia reservoir area in the Xunhua Basin, indicating that the climate in these two areas is a little warmer and more humid. In addition, the high mountain ranges in the study area have a blocking effect on the wind, which affects the deposition of clay minerals.

5. Discussion

5.1. The spatio-temporal distribution of giant landslides

Landslides are correlated in space and time, which is nowadays widely recognized (Soldati *et al.*, 2004; Sanchez *et al.*, 2010; Tonini and Cama, 2019). Using remote sensing interpretation and field investigation,

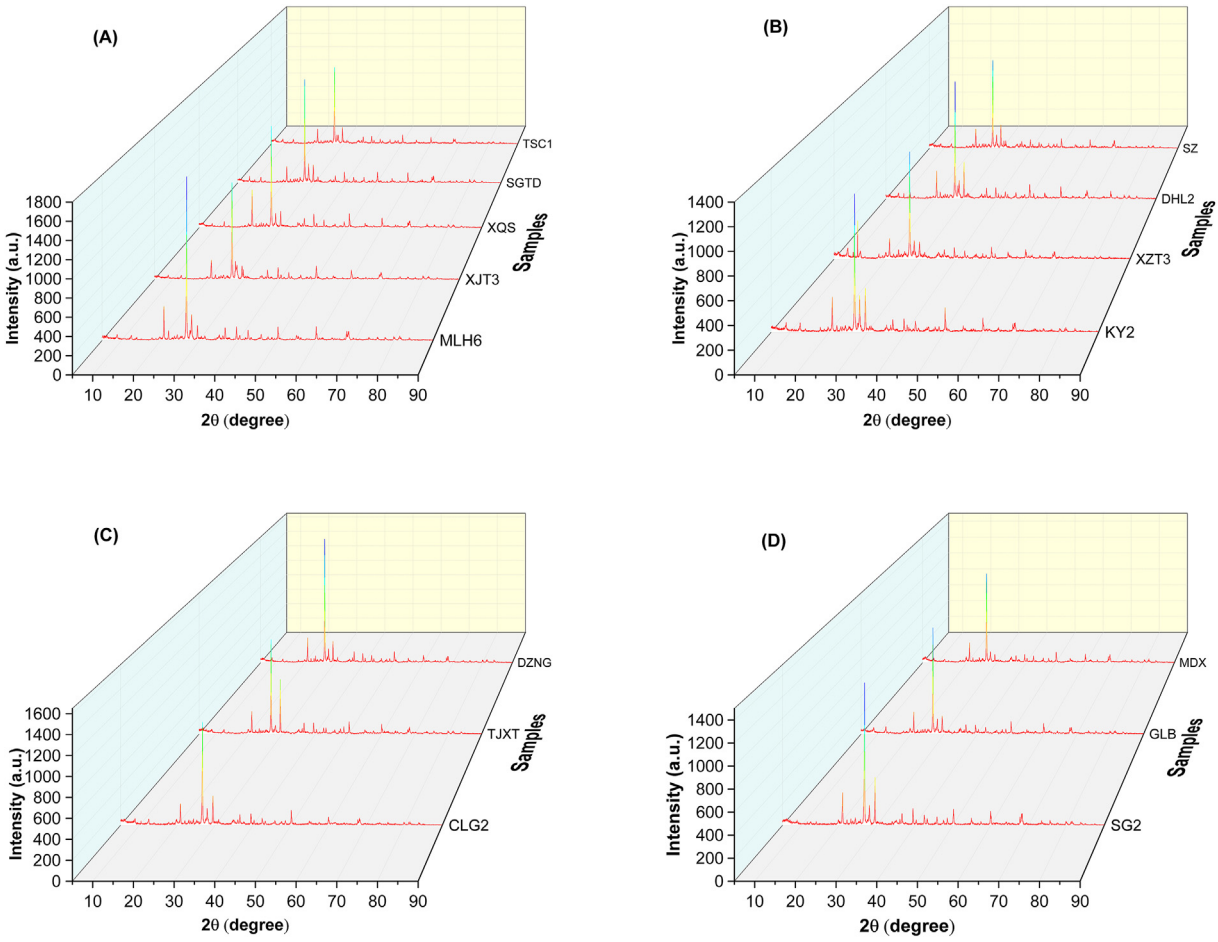

Fig. 7 3D waterfall diagram of deposits. **A)** 3D waterfall diagram of samples include MLH6, XJT3, XQS, SGTD and TSC1; **B)** 3D waterfall diagram of samples include KY2, XZT3, DHL2 and SZ; **C)** 3D waterfall diagram of samples include CLG2, TJXT and DZNG; **D)** 3D waterfall diagram of samples include SG2, GLB and MDX.

the basic features of giant landslides were identified (Fig. 8). According to their planar morphological characteristics, giant landslides can be mainly classified as chair-shaped, tongue-shaped, rectangular, winnowing fan-shaped, circular arc-shaped, and triangular (Yin *et al.*, 2016) (Fig. 9). Some giant landslides showed a chair shape, with a steeper crown and a head scarp slope of 12°—64°. The landslide toe is tongue-like or long tongue-like, part of the giant paleo-landslide accumulation, and the landslide toe suffered many times of erosion and transformation. The landslide scarp is better preserved, and the landslide deposit in the slope surface is as parts of the slippery body, in the foot of the slope at the distribution of the high rambling beach or the step ground.

Giant landslides in the upper reaches of the Yellow River are mainly distributed in the center of the sedimentary basin along the Yellow River, the right bank of the canyon area, and the right bank near the river valley, which is mainly due to the eccentric force of the earth's rotation that makes the river deflected to the right, and the lateral erosion and cutting effect of the river on the right bank is strengthened, which forms a critical surface in the leading edge of landslides, and landslides are formed under the action of a concentrated rainfall or a paleo-earthquake.

Based on the field investigation, reference to previous research, and remote sensing image interpretation, the length, width, slope, area of the giant landslide body, and other information were derived. Based on the frequency distribution of the above data, we describe the features of the landslides. The length range of giant landslides in the study area spanned a large range of lengths, mostly between 1300 m and 2700 m, with a minimum length of 1070 m and a maximum length of 8502 m. The width of landslides, mostly 1500 m—4500 m, spanned a large range as well, with a minimum width of 912 m and a maximum width of 8323 m (Fig. 10).

The statistics found that more landslides with lengths greater than widths are mostly in the shape of long tongues and chairs, mostly distributed on both

Table 4 The major element contents (wt. %) and maturity of samples from the upper Yellow River.

Sample	SiO_2	TiO_2	Al_2O_3	Fe_2O_3	MnO	MgO	CaO	Na_2O	K_2O	P_2O_5	LOI	Total	Maturity
MLH1	68.97	0.64	10.31	3.06	0.06	1.70	5.11	2.29	2.04	0.15	5.45	99.78	6.69
MLH4	62.82	0.62	12.15	4.03	0.08	2.06	6.05	1.98	2.36	0.15	8.02	100.32	5.17
MLH6*	67.11	0.57	10.71	3.06	0.06	1.59	5.73	2.17	2.07	0.14	6.62	99.83	6.27
XJT2*	61.01	0.70	11.26	3.98	0.08	2.69	7.24	2.00	2.31	0.20	8.75	100.22	5.42
XJT3	63.63	0.64	10.73	3.48	0.08	2.24	7.26	2.11	2.22	0.17	7.51	100.07	5.93
XQS	62.13	0.67	10.64	4.46	0.11	2.67	7.09	1.50	2.02	0.19	8.83	100.31	5.84
SGTD*	62.66	0.61	10.45	3.55	0.09	2.43	7.94	1.98	2.06	0.17	8.26	100.20	6.00
TSC1	57.23	0.58	11.52	3.97	0.08	2.55	8.84	1.55	2.30	0.15	10.88	99.65	4.97
KY2*	59.43	0.55	10.95	3.72	0.08	2.52	8.71	2.03	2.32	0.15	8.88	99.34	5.43
KY3	54.09	0.54	10.38	3.68	0.07	2.98	11.85	2.28	2.06	0.11	12.30	100.34	5.21
XZT2*	55.74	0.65	15.07	5.59	0.11	3.05	5.86	1.64	2.83	0.15	9.57	100.26	3.70
XZT3	59.04	0.70	13.73	5.08	0.07	2.53	5.21	2.02	2.61	0.16	8.96	100.11	4.30
DHL2	61.25	0.55	10.50	3.36	0.07	2.43	8.47	2.09	2.17	0.15	8.25	99.29	5.83
SZ	53.17	0.56	11.08	4.34	0.07	2.87	10.46	3.40	2.20	0.13	11.29	99.57	4.80
SG1*	60.85	0.52	9.92	3.11	0.06	1.88	9.32	1.52	1.75	0.11	10.37	99.41	6.13
SG2	60.25	0.55	9.48	2.94	0.04	1.92	10.48	1.86	1.85	0.09	10.37	99.83	6.36
CLG2	56.81	0.59	11.97	4.22	0.06	2.82	8.14	1.75	2.39	0.14	10.61	99.50	4.75
TJXT	57.94	0.56	11.11	3.39	0.06	1.92	9.72	1.62	2.10	0.11	11.08	99.61	5.22
DZNG	60.63	0.57	10.30	3.09	0.02	2.16	9.53	1.63	1.92	0.12	10.21	100.18	5.89
MDX	62.05	0.74	14.26	5.09	0.07	2.75	4.11	1.40	2.69	0.16	7.06	100.38	4.35
GLB	56.38	0.70	13.13	4.76	0.02	2.77	7.89	1.70	2.99	0.16	9.14	99.64	4.29

1) Samples* are from slope deposits in the Yellow River section.
2) Maturity = SiO_2/Al_2O_3.

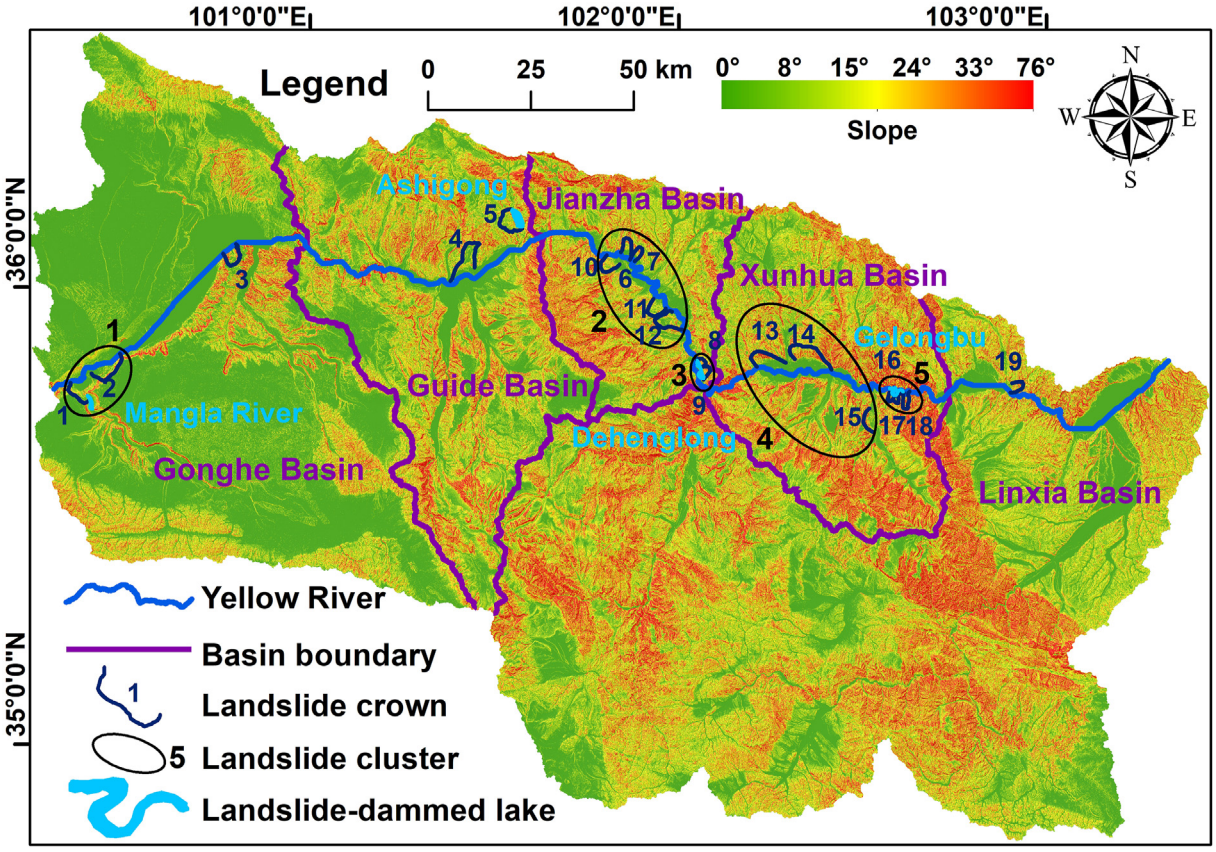

Fig. 8 Distribution of giant landslides in the upper reaches of the Yellow River.

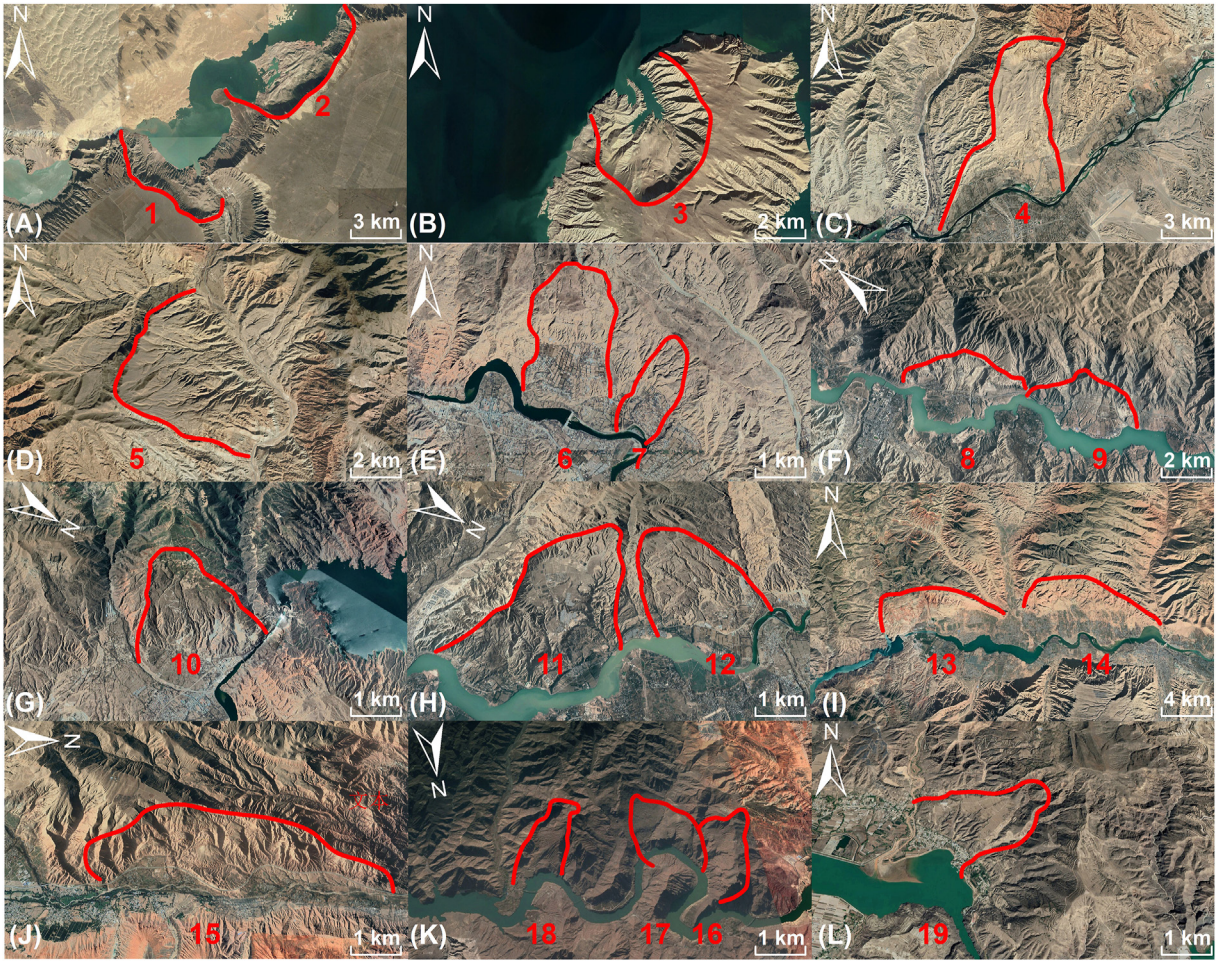

Fig. 9 Morphological characteristics of giant landslides in the upper reaches of the Yellow River (from Google Earth Pro). **A)** Mangla River and Baicitan landslides (winnowing fan-shaped) in the Gonghe Basin; **B)** Chana landslide (chair-shaped) in the Gonghe Basin; **C)** Xijitan landslide (rectangular) in the Guide Basin; **D)** Ashigong landslide (triangle) in the Guide Basin; **E)** Xiaqiongsi and Shenguotan landslides (tongue-shaped) in the Jianzha Basin; **F)** Dehenglong and Suozi landslides (circular arc-shaped) in the Jianzha Basin; **G)** Tangsecun landslide (triangle) in the Jianzha Basin; **H)** Kangyang and Xiazangtan landslides (rectangular) in the Jianzha Basin; **I)** Tangjiaxiantan and Chaligang landslides (circular arc-shaped) in the Xunhua Basin; **J)** Shangen landslide (circular arc-shaped) in the Xunhua Basin; **K)** Maerpodong landslide (tongue-shaped), Gelongbu and Mendaxiang landslides (triangle) in the Xunhua Basin; **L)** Badashan landslide (triangle) in the Linxia Basin.

sides of the mainstream of the Yellow River in the Jianzha Basin, which have a large difference from the landslides with large lengths formed in slope elevation and open frontage, such as Xiaqiongsi landslide (No. 6), Shenguotan landslide (No. 7), Kangyang landslide (No. 11), and Xiazangtan landslide (No. 12). These landslides belong to the category of giant landslides by volume, and belong to the category of mudstone landslides by the type of material composition, which have long sliding distances and huge sliding widths. These types of landslides also have relatively large sliding speeds, partially blocking the Yellow River, forming a huge landslide-dammed lake, and leaving landslide piles on the opposite bank of the Yellow River, such as the Dehenglong (No. 8), Suozi (No. 9), and Gelongbu (No. 17) landslides (Yin *et al.*, 2016). Some landslides belong to the creep-slip type, with short sliding distances and limited mobility, such as the Tangjiaxiantan landslide (No. 13) at the mouth of Gongbo Gorge. The landslides with a width greater than the length are mainly distributed in the Gonghe Basin and the Xunhua Basin, such as the Mangla River landslide (No. 1), the Baicitan landslide (No. 2), the Chaligang landslide (No. 14), and the Shangen landslide (No. 15). The Yellow River tributaries are generally narrower, with a limited frontage, and the wide-body landslides are developed. They belong to the semi-consolidated rock landslides, and they are mainly presented in the form of saddle shape and semi-curve shape on the planar morphology. Sliding distances of these types of landslides are relatively short, and the landslide crown is well preserved, upright and steep.

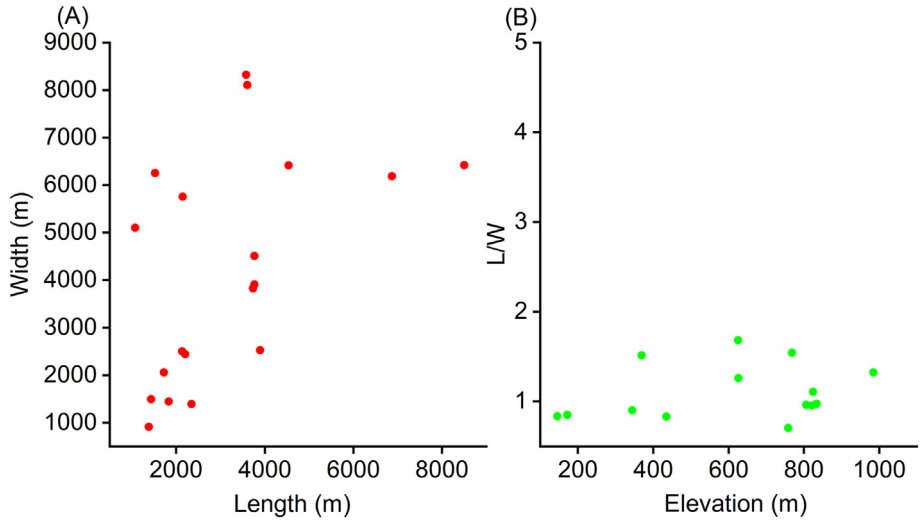

Fig. 10 **A)** Diagram of length versus width of giant landslides in the study area and **B)** Diagram of elevation versus length/width of giant landslides in the study area.

Giant landslides in the study area mostly occur along the Yellow River, with an uninterrupted and continuous distribution from Laganxia to Liujiaxia. They have the most intensive distribution in the Jianzha section, and the Mangla River landslide in the Gonghe Basin, the Ashigong landslide in the Guide Basin, and the Shangen landslide in the Xunhua Basin are located next to the tributaries of the Yellow River (Fig. 8). The continuous downcutting of the tributaries favors slope instability phenomena, and the occurrence of landslides may significantly impact the evolution of the river valley geomorphology.

The longitudinal profile of the Yellow River, exhibits three major knickpoints (Fig. 11B), which are located in Laxiwa Gorge, Gongbo Gorge, and Jishi Gorge. This spatial correspondence is not random and indicates that the Yellow River was formed by retrogressive erosion processes which progressively cut through the basins in succession. The section shows vertical steps corresponding to hydroelectric power plants that artificially modified the Yellow River profile. The interior of the Gonghe Basin is flat and little differential uplift has occurred. The slope drop of the Yellow River within the Guide Basin is the largest, and

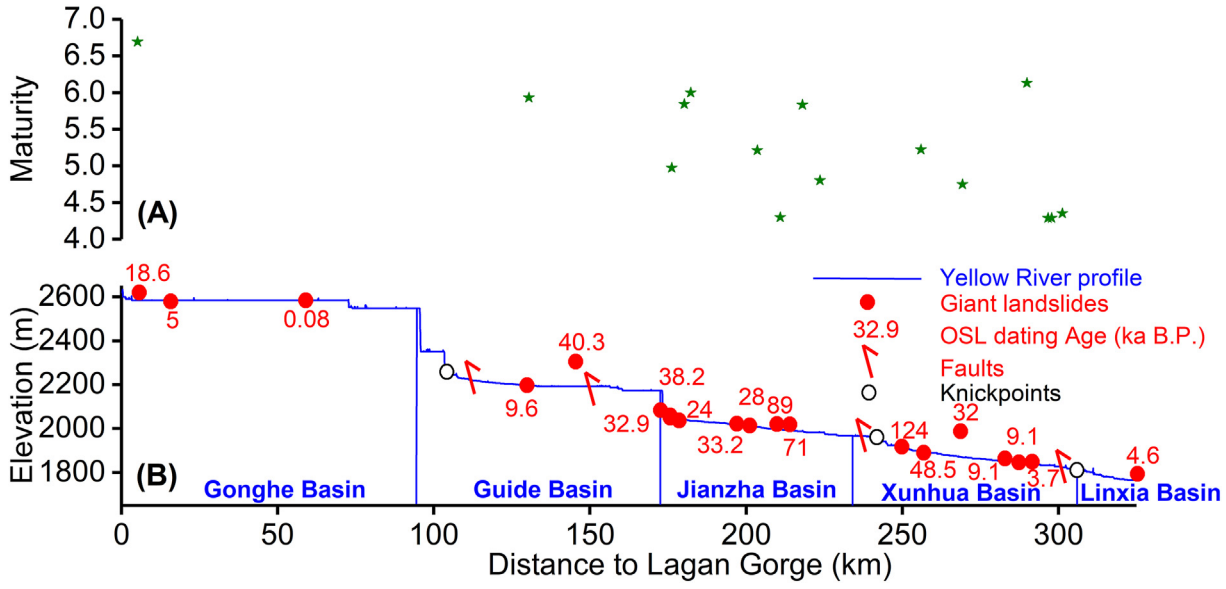

Fig. 11 **A)** The maturity of giant landslide deposits from upstream to downstream of the mainstream of the Yellow River (refer to Table 4); **B)** Longitudinal profile of the upper Yellow River from the Lagan Gorge to Liujia Gorge. Red dots are the locations of giant landslides. Profile was extracted from DEM (Fault location derived from Fig. 1).

in the west, the river drops steeply by more than 300 m. Therefore, the potential energy of the water flow in this section is the largest, and high and steep slopes of several hundred meters are formed. For example, the Xijitan landslide in the eastern part of the basin is characterized by large-scale and multi-phase development, and the landslide altered the channel to a certain extent to oscillate the flow direction many times; and there are now several oxbow lakes formed by the abandoned channel of the Yellow River. The landslide scale in the Jianzha Basin is the largest, with the most intensive river section distribution, but the slope descent ratio is not the lowest. The author suggests that the present-day river profile differs from that at the time of when the landslide occurred, reflecting the cumulative effects of repeated geomorphological changes prior to the landslide event. Along this section, the landslides have altered the original river profile, resulting in a relatively flat and regular present-day profile. The eastern boundary of the Xunhua Basin is marked by the junction of Laji Mountain and Jishi Mountain, where three bedrock landslides are distributed in the Jishi Gorge area. Previous studies indicate that this region has experienced multiple episodes of uplift since the Pleistocene (Yin *et al.*, 2016).

Based on the latest remote sensing data of the landslide deformation displacements, there is a possibility that some of the giant ancient landslides could be reactivated (Du *et al.*, 2023). According to the longitudinal profiles of the tributaries, the derived tributary knickpoints are all located upstream of the giant landslides, and the giant landslides are distributed in the concave banks of the tributaries, which indirectly confirms the important role of lateral erosion of the river in the landslide formation.

A few giant landslides are located next to the tributaries of the Yellow River, most are distributed along the mainstream. From a geomorphic perspective, they are primarily distributed at the low hills and steep slopes which are caused by tectonic erosion on the right bank of the mainstream of the Yellow River. From a temporal perspective, they are mainly concentrated in the periods from 40 ka to 24 ka and from 10 ka to 5 ka, which correspond to the periods of interglacial or glacial-to-interglacial transitions.

5.2. *Relationship between river-blocking events and lacustrine deposits*

Multiple landslide-dammed lakes were formed at some points in the past in such large scales. The results of previous research (Yin *et al.*, 2014; Guo *et al.*, 2015, 2020, 2022) indicate that four landslide-dammed lakes have occurred within the river reaches from Lagan Gorge to Liujia Gorge: Mangla River landslide-dammed lake, Ashigong landslide-dammed lake, Dehenglong landslide-dammed lake, and Gelongbu landslide-dammed lake, from west to east (Fig. 8), which means that at least four river-blocking events have occurred within the reach. The formation ages of these four landslide-dammed lakes are 18.6±2.7 ka, 40.3±2.7 ka, 89±8 ka, and 9.1 ka, respectively (Table 2), and all of them were formed as a result of the blockage of the river by the giant landslides at their locations, which have been estimated to cover an area of 0.38 km^2, 6 km^2, 460 km^2, and 128 km^2. The four landslide-dammed lakes are located far apart, and the distance between different landslide-dammed lakes along the mainstream of the Yellow River is 70 km—140 km. Due to their differences in spatio-temporal scales, there is no obvious evidence for showing that these lakes interact with each other, and it can be determined that these lakes exist independently. There is no potential for the formation of multiple landslide-dammed lakes by a single giant landslide. Each landslide-dammed lake was caused by a landslide blocking the river at that location. Lacustrine deposits are present upstream of all four landslide-dammed lakes in the river reach. Based on the field survey and sediment grain size analysis (Fig. 6), the profile has a typical lacustrine texture layer as well as lacustrine deposits.

Since the grain size distribution curves of the lacustrine deposits do not have a specific pattern, and there are several single-peak, double-peak, or multi-peak patterns of grain size distribution, the deposition or transport process of the lacustrine deposits needs to be further discussed (Fig. 6). The median grain size of the dominant component of the red clay sediments on the right bank of the Yellow River on the secondary terrace in the Xunhua Basin is generally smaller than that of the lacustrine deposits in the Gonghe Basin (Yin *et al.*, 2016), reflecting the different hydrodynamic conditions, transport modes, and transport distances in different sections of the upper Yellow River. The major elements in the lacustrine deposits differ from those in the landslide deposits, especially the Al_2O_3, Fe_2O_3, and MgO contents, which suggests that the particles in the lacustrine deposits are not of local origin. In the past, some scholars used the SiO_2/Al_2O_3 ratio as an indicator of the maturity of clastic sediments, and the gradual enrichment of quartz during the natural transport process would lead to an increase in the SiO_2/Al_2O_3 ratio. In general, the greater the maturity, the farther the transport distance from the source area is (Roser and Korsch, 1999). This is of great significance for understanding the giant landslide blockage event in

the upper Yellow River, the formation mechanism of the landslide-dammed lake, and the process of lacustrine deposit transport and accumulation. Other researchers concluded that when the maturity degree is greater than 4.3, the sediment can be considered to be of high maturity (Wang *et al.*, 2015). The maturity degree of lacustrine deposits are basically greater than 4.3, ranged from 4.29 to 6.69 (Table 4; Fig. 11A), which indicates that the lacustrine deposits have relatively higher maturity and longer transport distance, thus ruling out that the lacustrine deposits were made by the river erosion of local wind-formed sediments, and also proving the strong transport ability of the Yellow River on the deposits from the other side. From the upstream to the downstream of the mainstream of Yellow River, the maturity of giant landslide deposits is inversely proportional to the distance from the upstream and is decreasing, and the maturity of deposits in tributaries is higher than that in the mainstream, reflecting that the deposits in tributaries are subjected to long-distance transportation.

5.3. The genesis mechanism of giant landslides

Paleo-landslides are often related to the geological and geomorphological setting of the study area. Fundamental factors, such as climate, and triggering factors, such as heavy rainfall events and earthquakes, cause landslide occurrences. Comparative analyses of the temporal distribution of landslides in the region can be conducted to determine possible relationships between the landslide and climate changes during the glacial period and the interglacial period (Fig. 3). Most of the giant paleo-landslides in the upper Yellow River occurred during the interglacial periods and or the transition from the last glacial period to the interglacial period when the temperature rised and rainfall increased.

Paleoclimatic changes in the upper reaches of the Yellow River indicate that the peak of the warm period occurred between 80,000 and 75,000 years after the Marine Isotope Stage (MIS)-5a. Between 80,000 and 75,000 years, temperatures were about 3 °C higher than the modern climate. Beginning around 40,000 years ago, the precipitation increased, and temperatures in the northeastern Qinghai—Tibet Plateau were about 2°C—4°C higher than at present, corresponding to the late MIS-3 of the last glacial period. Finally, at around 10,000 years, there was an abrupt climate change that resulted in a significant increase in precipitation and temperature (Fig. 3). By comparing the giant landslide dating results and the records of paleoclimate changes, it can be hypothesized that the formation of giant landslides in the region is a response to the climatic changes that occurred since the transition from the last glacial to interglacial period or the interglacial period, and, a warmer climate in the region is generally associated to more severe rainfall and increased pace of river downcutting. The study area was characterized by active seismic faults and frequent paleo-earthquakes during this period. Both factors exert a detrimental effect on slope stability and are believed to represent the main controlling factors for the formation and development of giant landslides.

Based on the concentration of giant landslides in their spatio-temporal distribution, the study area can be roughly divided into five landslide clusters: 1) the Longyangxia Reservoir cluster, 2) the Jianzha Basin cluster, 3) the Gongbo Gorge cluster, 4) the Xunhua Basin cluster, and 5) the Jishi Gorge cluster (Fig. 8).

1) The Longyangxia Reservoir cluster

The Longyangxia Reservoir cluster is made up of Mangla River, and Baicitan landslides (Figs. 8,9A), which was occurred around 18 ka ago, probably in response to the warm and humid climate period associated with rainfall increase and the water level rise in the reservoir and tributaries as well. Eventually, a soft structural surface was formed at the bottom of the slope, and the foot of the slope began to creep and slip and deform. The occurrence of a paleo-earthquake made the sliding force greater than the slip resistance of the locked section, and the landslideslid sharply, then the landslide landform was formed.

2) The Jianzha Basin cluster

The Jianzha Basin cluster is made up of Xiaqiongsi, Shenguotan, Tangsecun, Kangyang, and Xiazangtan landslides (Figs. 8, 9E, 9G, 9H) involving mainly loess and mudstone. The climate of the Tibet Plateau was warm and humid during this period, which can be described as a “period of high temperatures and heavy precipitation”, with an intensification of the monsoon winds and a significant increase in precipitation to interglacial proportions. The majority of the Jianzha Basin cluster occurred 40 ka—20 ka ago, and was possibly related to the climate condition.

3) The Gongbo Gorge cluster

The Gongbo Gorge cluster is made up of the Dehenglong and Suozi landslides (Figs. 8 and 9F), which

are gneiss landslides. It occurred during 80 ka—70 ka due to the paleo-earthquake.

4) The Xunhua Basin cluster

The Xunhua Basin cluster is made up of Tangjiaxiantan, Chaligang and Shangen landslides (Figs. 8, 9I and 9J), which are red-layer landslides, and occurred mainly between 30 ka and 10 ka ago and derived from a response to the climate.

5) The Jishi Gorge cluster

The Jishi Gorge cluster is made up of Maerpodong, Gelongbu and Mendaxiang landslides (Figs. 8 and 9K), which are the sand and gravel landslides. It occurred around 10 ka due to the paleo-earthquake.

Faults affect landslides through earthquake vibration, and most giant landslides are located at some distance from the seismic faults. Ground vibration decay, as well as the peak seismic acceleration at the site where the giant landslides are considered to determine whether or not a landslide can occur. The fact that the landslide cannot slide beyond the limiting equilibrium in the saturated state and that it can only slide when a corresponding seismic load is applied proves the role played by paleoseismicity in the sliding of giant landslides. Combined with the paleoclimate fluctuation curves, the giant landslides occurred during the interglacial period or the transitional period from cold to warm, when the climate shifted from cold-dry to humid. The recurrence cycle of active faults is generally 2000—3000 years, however, the existing research data and information show that the time interval of the giant landslides does not coincide with the recurrence cycle of active faults, which proves that the giant landslides are not synseismic landslides, and there must be precipitation involved in their formation. Due to the serious lack of paleoseismic data in the study area, the accurate paleoseismic sequences of 10 ka ago have not been established yet, so it is impossible to compare the paleoseismicity with the paleoclimate.

The genesis mechanism of the giant landslides in the upper reaches of the Yellow River is the coupling effect of the paleoseismicity and precipitation (shown in Fig. 12), and the process of evolution is as follows: **A)** The uplift of the Tibet Plateau caused by the extrusion between the Indian Plate and the Eurasian Plate; **B)** The uplift of the geologic body that gave birth to the giant landslides to a certain height, and at the same time, the Yellow River started flowing through the whole study area and forming a high steep foot of the river bank due to continuously downcut; **C)** The Yellow River continued to downcut, and a series of internal and external dynamics, such as the fracture activity, weathering and denuding, and precipitation, made the slope body produce a number of joints and tension cracks; **D)** The Yellow River continued to downcut and the precipitation seeped into the slope along the tension cracks, forming gullies on both sides of the slope and forming a weak sliding surface within

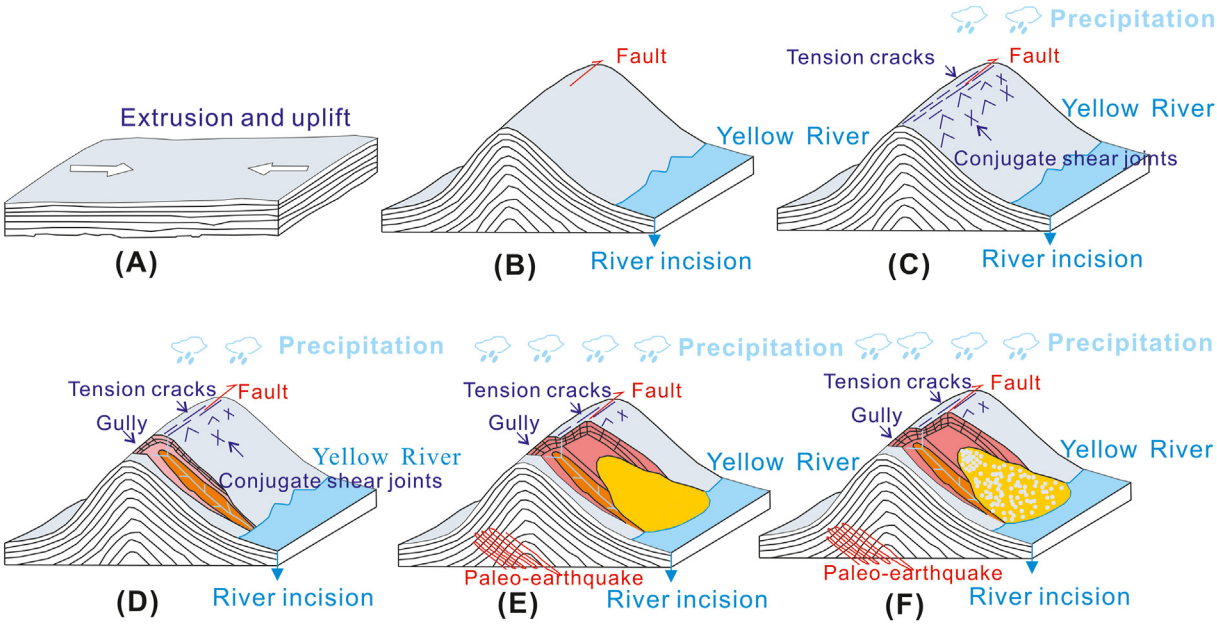

Fig. 12 Diagrams illustrating the formation and evolution pattern of a giant landslide distributed in the upper reaches of the Yellow River.

the slope; **E)** The Yellow River continued to downcut. Rainfall increased at the same time, and the water seeped into the slope for a long period, caused the slope to reach a saturated state. An earthquake is formed by a nearby seismic fault, and the ground vibration propagated to the site of the giant landslide; the limit equilibrium state of the giant landslide is destroyed; **F)** Continued ground shaking has linked up the potential sliding surface of the giant landslides, and the landslides have collapsed and disintegrated into blocks of varying grain sizes, which rushed across the opposite bank of the Yellow River under the powerful energy of the paleo-earthquake, blocking the Yellow River to form a landslide-dammed lake.

6. Conclusions

This study used chronological datas from OSL dating results and other related articles and theoretical analysis to reveal the genesis mechanism of the giant landslides in the upper reaches of the Yellow River, which is response to the coupling effect of tectonic activity and paleoclimate. In particular, tectonic activity and paleoclimate determine the factors triggering giant landslides such as paleoseismicity and precipitation in the study area, while influencing the downcut and evolution of the upper reaches of the Yellow River. The study has reference significance to the giant landslides beside large rivers, in the following respects:

1) All the giant landslides were mapped through the field investigation and the interpretation of remote sensing data, and 90% of the giant landslides are located in the upper reaches of the Yellow River.
2) There are at least four ancient landslide-dammed lakes in the upper reaches of the Yellow River from Lagan Gorge to Liujia Gorge. All of them existed independently, and had not affected each other on the spatial and temporal scales.
3) The results of the element analyses indicated that the chemical composition of the lacustrine deposits is very different from that of the local sediments, suggesting that the lacustrine deposits are not of a local origin. Thus, the Yellow River had a strong transport capacity during the formation period of the lacustrine deposits.
4) The giant landslides in the upper reaches of the Yellow River could be divided into five major clusters mainly due to the paleoclimate and paleoseismic activity.

CRediT authorship contribution statement

Yi-Qi Ji: Writing — original draft, Visualization, Validation, Software, Methodology, Investigation, Formal analysis, Data curation, Conceptualization. **Sheng-Rui Su:** Writing — review & editing, Supervision, Conceptualization. **Alessandro Simoni:** Writing — review & editing, Methodology, Conceptualization. **Qiang-Bing Huang:** Resources, Project administration, Funding acquisition.

Availability of data and materials

Data supporting the findings of this study are available upon request from the corresponding author.

Funding

This work was supported by the National Natural Science Foundation of China (Grant No. 42041006) and the China Scholarship Council Studentship Awarded to Yi-Qi Ji (Ref. 202206560049).

Declaration of competing interest

The authors declare that they have no known competing financial interests or personal relationships that could have appeared to influence the work reported in this paper.

Acknowledgements

The authors greatly appreciate anonymous reviewers for their constructive comments and thanks to Dr. Ze-Hua Zhou for helping in the fieldwork.

References

An, F.Y., Ma, H.Z., Wei, H.C., Lai, Z.P., 2012. Distinguishing aeolian signature from lacustrine sediments of the Qaidam Basin in northeastern Qinghai—Tibetan Plateau and its palaeoclimatic implications. *Aeolian Research*, 4, 17—30.

Chigira, M., 2002. Geologic factors contributing to landslide generation in a pyroclastic area August l998 Nishigo Village, Japan. *Geomorphology*, 46, 117—128.

Cordier, S., Briant, B., Bridgland, D., Herget, J., Maddy, D., Mather, A., Vandenberghe, J., 2017. The Fluvial Archives Group: 20 years of research connecting fluvial geomorphology and palaeoenvironments. *Quaternary Science Reviews*, 166, 1—9.

Du, J.T., Li, Z.H., Song, C., Zhu, W., Ji, Y.Q., Zhang, C.L., Chen, B., Su, S.R., 2023. InSAR-based active landslide detection and characterization along the upper reaches of the Yellow River. *Ieee Journal of Selected Topics in Applied Earth Observations and Remote Sensing*, 16, 3819—3830.

Folk, R.L., Ward, W.C., 1957. Brazos River bar: A study in the significance of grain size parameters. *Journal of Sedimentary Research*, 27, 3—26.

Guo, X.H., Forman, S.L., Marin, L.M., Li, X.L., 2018. Assessing tectonic and climatic controls for Late Quaternary fluvial terraces in Guide, Jianzha, and Xunhua basins along the Yellow River on the northeastern Tibetan Plateau. *Quaternary Science Reviews*, 195, 109—121.

Guo, X.H., Lai, Z.P., Lu, Y.D., Li, X., Sun, Z., 2015. Optically stimulated luminescence (OSL) chronology of the Dehenglong Landslide from Longyang Gorge to Liujia Gorge along Upper Yellow River, China. *Acta Geologica Sinica (English Edition)*, 9(1), 242—250.

Guo, X.H., Wei, J.C., Song, Z.J., 2022. Luminescence dating of a dammed lake formed by Ashegong landslide on the northeastern Tibetan Plateau. *Quaternary International*, 629, 74—80.

Guo, X.H., Wei, J.C., Song, Z.J., Lai, Z.P., Yu, L.P., 2020. Optically stimulated luminescence chronology and geomorphic imprint of Xiazangtan landslide upon the upper Yellow River valley on the northeastern Tibetan Plateau. *Geological Journal*, 55, 5498—5507.

Huntley, D.J., Prescott, J.R., 2001. Improved methodology and new thermoluminescence ages for the dune sequence in south—east South Australia. *Quaternary Science Reviews*, 20(5—9), 687—699.

Ji, Y.Q., 2024. *Tectonic geomorphology and genetic mechanism of giant landslides from Lagan Gorge to Liujia Gorge in the upper reaches of the Yellow River*. Chang'an University. Ph.D. Thesis.

Ji, Y.Q., Su, S.R., Huang, Q.B., 2022. Active tectonics in the upper reaches of the Yellow River from Lagan Gorge to Liujia Gorge, northwestern China: Insights from geomorphic indices. *Geological Journal*, 57(6), 2379—2396.

Ji, Y.Q., Su, S.R., Liu, Z.H., Huang, Q.B., 2021. Assessment of tectonic activity based on the geomorphic indices in the middle reaches of the upstream of Jinsha River, China. *Geological Journal*, 56(8), 3974—3991.

Kumar, V., Gupta, V., Sundriyal, Y.P., 2019. Spatial interrelationship of landslides, litho-tectonics, and climate regime, Satluj valley, Northwest Himalaya. *Geological Journal*, 54, 537—551.

Lan, H.X., Peng, J.B., Zhu, Y.B., Li, L.P., Pan, B.T., Huang, Q.B., Li, J.H., Zhang, Q., 2022. Geological and surfacial processes and major disaster effects in the Yellow River Basin. *Science China Earth Sciences*, 62(2), 234—256.

Li, J.J., Zhou, S.Z., Zhao, Z.J., Zhang, J., 2015. The Qingzang movement: The major uplift of the Qinghai—Tibetan Plateau. *Science China Earth Sciences*, 58, 2113—2122.

Li, X.L., Guo, X.H., Li, W.L., 2011. Mechanism of giant landslides from Longyangxia valley to Liujiaxia valley along upper Yellow River. *Journal of Engineering Geology*, 19(4), 516—529 (in Chinese with English Abstract).

Li, X., Li, S.D., Chen, J., Liao, Q.L., 2008. Coupling effect mechanism of endogenic and exogenic geological processes of geological hazards evolution. *Chinese Journal of Rock Mechanics and Engineering*, 27(9), 1792—1807, 2008(in Chinese with English Abstract).

Li, Y.C., Chen, J.P., Tan, C., Gu, F.F., Zhang, Y.W., Ammar, M., Wang, Q., 2022. Implications of the discovery of rapidly deposited lacustrine sediments in the Suwalong reach of the upper Jinsha River, SE Tibetan Plateau. *Bulletin of Engineering Geology and the Environment*, 81(12), 497.

Li, Y.C., Chen, J.P., Zhou, F.J., Song, S.Y., Zhang, Y.W., Gu, F.F., Cao, C., 2020. Identification of ancient river-blocking events and analysis of the mechanisms for the formation of landslide dams in the Suwalong section of the upper Jinsha River, SE Tibetan Plateau. *Geomorphology*, 368, 107351.

Liu, Z.H., Han, L., Yang, Z.H., Cao, H.Y., Guo, F.C., Guo, J.H., Ji, Y.Q., 2021. Evaluating the vertical accuracy of DEM generated from ZiYuan-3 stereo images in understanding the tectonic morphology of the Qianhe Basin, China. *Remote Sensing*, 13, 1203.

Martinson, D.G., Pisias, N.G., Hays, J.D., Imbrie, J., Moore, T.C., Shackleton, N.J., 1987. Age dating and the orbital theory of the ice ages: Development of a high-resolution 0 to 300,000-year chronostratigraphy. *Quaternary Research*, 27, 1—29.

Qin, X.G., Mu, Y., Ning, B., Yin, Z.Q., 2009. Climate effect of dust aerosol in southern Chinese Loess Plateau over the last 140,000 years. *Geophysical Research Letters*, 36(2), L02707.

Roser, B.P., Korsch, R.J., 1999. Geochemical characterization, evolution and source of a Mesozoic accretionary wedge: The Torlesse terrane, New Zealand. *Geological Magazine*, 136(5), 493—512.

Roser, B.P., Korsch, R.J., 1988. Provenance signatures of sandstone—mudstone suites determined using discriminant function analysis of major-element data. *Chemical Geology*, 67, 119—139.

Sanchez, G., Rolland, Y., Corsini, M., Braucher, R., Bourlès, D., Arnold, M., Aumaître, G., 2010. Relationships between tectonics, slope instability and climate change: Cosmic ray exposure dating of active faults, landslides and glacial surfaces in the SW Alps. *Geomorphology*, 117(1—2), 1—13.

Shanmugam, G., 2015. The landslide problem. *Journal of Palaeogeography*, 4(2), 109—166.

Shi, Y.F., Li, J.J., Li, B.Y., Yao, T.D., Wang, S.M., Li, S.J., Cui, Z.J., Wang, F.B., Pan, B.T., Fang, X.M., Zhang, Q.S., 1999. Uplift of the Qinghai—Xizang (Tibetan) Plateau and East Asia environmental change during Late Cenozoic. *Acta Geographica Sinica*, 54(1), 10—20 (in Chinese with English Abstract).

Soldati, M., Corsini, A., Pasuto, A., 2004. Landslides and climate change in the Italian Dolomites since the Late Glacial. *Catena*, 55(2), 141—161.

Tonini, M., Cama, M., 2019. Spatio-temporal pattern distribution of landslides causing damage in Switzerland. *Landslides*, 16, 2103—2113.

Wang, C.L., Zhang, L.C., Dai, Y.P., Lan, C.Y., 2015. Geochronological and geochemical constraints on the origin of clastic meta-sedimentary rocks associated with the Yuanjiacun BIF from the Lüliang Complex, North China. *Lithos*, 212—215, 231—246.

Wang, Y.J., Cheng, H., Edwards, R.L., Kong, X.G., Shao, X.H., Chen, S.T., Wu, J.Y., Jiang, X.Y., Wang, X.F., An, Z.S., 2008. Millennial- and orbital-scale changes in the East Asian monsoon over the past 224,000 years. *Nature*, 451, 1090—1093.

Yao, T.D., Shi, Y.F., Qin, D.H., Jiao, K.Q., Yang, Z.H., Tian, L.D., Thompson, L.G., Mosley-Thompson, E., 1997. A study on the climate changes from Guliya ice core records since last interglacial period. *Science China (Series D)*, 27(5), 447—452 (in Chinese with English Abstract).

Yin, K.L., Han, Z.S., Li, Z.Z., 2000. Progress of landslide researches in the world. *Hydrogeology & Engineering Geology*, 5, 1—4 (in Chinese with English abstract).

Yin, Z.Q., Qin, X.G., Yin, Y.P., Zhao, W.J., Wei, G., 2014. Landslide developmental characteristics and response to climate change since the last glacial in the upper reaches of the Yellow River, NE Tibetan Plateau. *Acta Geologica Sinica (English Edition)*, 88, 635—646.

Yin, Z.Q., Qin, X.G., Zhao, W.J., Li, X.L., Chen, G.M., Wei, G., Shi, L.Q., Yuan, C.D., 2016. *Spatial and temporal evolution and triggering mechanism of landslides and debris flows in the upper Yellow River*. Science Press, Beijing, pp. 89—166 (in Chinese).

Zhang, D.F., Liu, F.Q., Bing, J.M., 2000. Eco-environmental effects of the Qinghai—Tibet Plateau uplift during the Quaternary in China. *Environmental Geology*, 39, 1352—1358.

Zhou, B., Peng, J.B., Lai, Z.P., Fu, C.F., Lin, H.Z., Zhao, R.X., 2014. Research on geochronology of super large landslide in the upper Yellow River. *Quaternary Sciences*, 34(2), 346—353 (in Chinese with English Abstract).